

PÄÄRN PAISTE

Geopolymeric potential of the Estonian
oil shale processing waste



PÄÄRN PAISTE

Geopolymeric potential of the Estonian
oil shale processing waste



UNIVERSITY OF TARTU
Press

Department of Geology, Institute of Ecology and Earth Sciences, Faculty of Science and Technology, University of Tartu, Estonia.

This dissertation is accepted for the commencement of the degree of Doctor of Philosophy in Geology at the University of Tartu on the 8th of May 2017 by the Scientific Council of the Institute of Ecology and Earth Sciences, University of Tartu.

Supervisors: Kalle Kirsimäe
Department of Geology, University of Tartu, Estonia

Riho Mõtlep
Department of Geology, University of Tartu, Estonia

Opponent: Miroslav Komljenović
Research Professor, Institute for Multidisciplinary Research,
University of Belgrade, Serbia.

This thesis will be defended at the University of Tartu, Estonia, Chemicum, Ravila 14A, room 1019, on the 30th of June 2017 at 12:15.

Publication of this thesis is granted by the Institute of Ecology and Earth Sciences, University of Tartu and by the University of Tartu ASTRA Project PER ASPERA Doctoral School of Earth Sciences and Ecology (2014-2020.4.01.16-0027), created under the auspices of the European Regional Development Fund.



European Union
European Regional
Development Fund



Investing
in your future

ISSN 1406-2658
ISBN 978-9949-77-451-7 (print)
ISBN 978-9949-77-452-4 (pdf)

Copyright: Päärn Paiste, 2017

University of Tartu Press
www.tyk.ee

CONTENTS

ABBREVIATIONS.....	6
LIST OF ORIGINAL PUBLICATIONS	7
1. INTRODUCTION.....	8
2. ESTONIAN OIL SHALE AND ITS SOLID PROCESSING RESIDUES.....	10
2.1. Thermal power plant residues.....	11
2.2. Shale oil retorting residues	11
3. MATERIALS AND METHODS	14
3.1. Ash materials.....	14
3.2. Experimental design and sample preparation.....	14
3.3. Analytical methods.....	15
4. RESULTS AND DISCUSSION	17
4.1. Thermal power plant residues.....	17
4.1.1. Phase composition and microstructure	17
4.1.2. Structural characteristics of geopolymerization.....	18
4.1.3. Strength development	20
4.2. Petroter type solid heat carrier shale oil pyrolysis residues.....	20
4.2.1. Phase composition and microstructure	20
4.2.2. Structural characterization of geopolymerization processes in SHC black ash mixtures	23
4.2.3. Strength development	26
4.3. Enefit280 type solid heat carrier shale oil pyrolysis residues.....	27
4.3.1. Phase composition and microstructure	27
4.3.2. Structural characterization of geopolymerization processes in SHC WHB ash mixtures	28
4.3.3. Strength development	29
5. GEOPLOYMERIC POTENTIAL OF ESTONIAN OIL SHALE PROCESSING RESIDUES	31
6. CONCLUSIONS.....	35
REFERENCES.....	37
SUMMARY IN ESTONIAN	43
ACKNOWLEDGEMENTS	47
PUBLICATIONS	49
CURRICULUM VITAE	120
ELULOOKIRJELDUS.....	122

ABBREVIATIONS

^{29}Si MAS-NMR	silicon magic angle spinning nuclear magnetic resonance spectroscopy
APS	ash plateau sediment
ATR-FT-IR	attenuated total reflectance – Fourier transform infrared spectroscopy
BA	furnace bottom ash
CA	cyclone separator ash
C-A-H	calcium-aluminium-hydrate
C-A-S-H	calcium-aluminium-silicate-hydrate
CFB	circulating fluidized bed
C-S-H	calcium-silicate-hydrate
DTA	differential thermal analysis
L.O.I.	loss on ignition
MAS-NMR	magic angle spinning nuclear magnetic resonance spectroscopy
Na-silicate	sodium silicate solution with $\text{SiO}_2/\text{Na}_2\text{O}$ molar ratio of 2.72
Na-silicate/NaOH	sodium silicate solution modified by sodium hydroxide addition to $\text{SiO}_2/\text{Na}_2\text{O}$ molar ratio 1.5
NMR	nuclear magnetic resonance spectroscopy
PAH	polycyclic aromatic hydrocarbons
PF	pulverized firing
SEM	scanning electron microscopy
SEM-EDS	scanning electron microscopy with energy-dispersive X-ray spectroscopy
SHC	solid heat carrier
TGA	thermogravimetric analysis
TMS	Tetramethylsilane
TPP	thermal power plant
WHB	waste heat boiler
XRD	X-ray diffraction
XRF	X-ray fluorescence spectrometry

LIST OF ORIGINAL PUBLICATIONS

This thesis is based on the following published and submitted papers, which are referred to in the text by their Roman numerals. The papers are reprinted by kind permission of the publishers.

- I Paiste, P.**, Liira, M., Heinmaa, I., Vahur, S., Kirsimäe, K. (2016) Alkali activated construction materials: Assessing the alternative use for oil shale processing solid wastes. *Construction and Building Materials* 122, 458–464,
- II Paaver, P., Paiste, P.**, Kirsimäe, K. (2016) Geopolymeric potential of the Estonian oil shale solid residues: Petroter solid heat carrier retorting ash. *Oil Shale* 33, 373–392.
- III Paiste, P.**, Külaviir, M., Paaver, P., Heinmaa, I., Vahur, S., Kirsimäe, K. (2017) Beneficiation of oil shale processing waste: secondary binder phases in alkali activated composites. *Waste and Biomass Valorisation* submitted, in review
- IV Paaver, P., Paiste, P.**, Mötlep, R., Kirsimäe, K. (2017) Self-cementation properties and alkali activation of Enefit280 solid heat carrier retorting ash. *Oil Shale* 34, in press.

Author's contribution:

Paper I: The author was responsible for planning original research, data collection, participated in mineralogical-geochemical-structural data analysis and interpretation of analytical results, synthesis of analytical data and writing of the manuscript.

Paper II: The author was responsible for planning research, running experiments, data collection, and contributed to the writing of the manuscript.

Paper III: The author was primarily responsible for planning original research, participated in data collection and interpretation of analytical results, synthesis of mineralogical-geochemical-structural data and coordinated the writing of the manuscript.

Paper IV: The author was responsible for planning research, running experiments, data collection, and contributed to the writing of the manuscript

1. INTRODUCTION

Geopolymers, also referred as inorganic polymers, are three-dimensionally structured aluminosilicate binders formed at low temperature and short time by alkali activation of naturally occurring aluminosilicate precursors [1]. Formation of geopolymers occurs when aluminosilicate raw material is dissolved in alkaline solution, and aluminate and silicate species are released into aqueous phase forming a complex colloidal solution of silicate, aluminate and aluminosilicate species. In supersaturated solution a gel is formed and aluminosilicate oligomers form networks that, while having non-stoichiometric composition and comprise mixtures of amorphous to semi-crystalline structure and crystalline Al–Si particles.

Geopolymers are cementitious materials that can provide the mortar and concrete with mechanical performance similar to ordinary Portland cement system, are of high fire and acid resistance, and can be used to stabilize/solidify different wastes including heavy metals [2]. It is also pivotal that the production of geopolymeric binders is, compared with ordinary Portland cement, ca. 60% more energy-efficient and the associated carbon dioxide emissions can be up to 80% lower [3]. Geopolymeric binders can be produced from any naturally occurring or industrially produced aluminosilicate raw materials, such as as (kaolin)clay or blast furnace slag from steel industry [1]. Secondary usage of different industrial by-products and solid wastes as precursors of geopolymeric binders is specifically beneficial and can significantly reduce the amount of the industrial waste otherwise landfilled/deposited.

The raw materials and their processing conditions determine the structure, chemical and physical properties of formed geopolymeric products. In macroscopic scale, geopolymers synthesised from different aluminosilicate sources may appear similar but their microstructure homogeneity and thus the physical, mechanical and also chemical properties vary to a large extent [4]. In addition to different types of slags and the waste from glass manufacturing industry, combustion fly ash, a widespread industrial waste, can also be potentially useful for production of geopolymeric alkali activated materials. Commonly class F type low-Ca fly ash is used for geopolymeric binder production [5]. However, also class C i.e. high-Ca fly ashes have been successfully tested for geopolymeric binder production [6–8]. Valorisation of different solid industrial wastes through alkali activation promoting the formation of secondary polymeric silicate binder phases that lead to improved cementitious properties of the subject material, is recognized as one of the most viable options for the reuse of these types of wastes [9,10]

In Estonia, more than 70% of the energy sector relies on the mining and processing of Ordovician marine kerogenous oil shale [11]. Estonian oil shale industry is the largest oil shale processing operation in the world today and at current production rates ca. 19 Mt of oil shale is mined annually and mostly used at thermal power plants for electricity and heat (ca. 80% of the mined

shale) whereas ca. 19% of mined oil shale is used for retorting shale oil and shale gas [12]. Oil shale is a Ca-rich solid fuel of low calorific value and ca. 40–50 wt% of the processed shale remains as a solid waste, majority of which (~98%) becomes landfilled. Only the finest fractions of the fly ash from thermal power plants with lime (CaO_{free}) content less than 10% are used as an additive to Portland cement, whereas solid residues from shale oil retorting are currently not used in any beneficial purpose and are landfilled [13,14].

It is therefore important to find sustainable uses for oil shale solid residues and synthesising geopolymeric materials potentially used in building-construction industry could be one of the viable options. Reuse of this waste would also help to reduce the overall CO_2 footprint and energy consumption of the oil shale industry that is responsible for producing more than 70% of the CO_2 emissions in Estonia [15].

This thesis studies the geopolymerization potential of different Ca-rich Estonian oil shale processing residues: (1) the oil shale ash produced in Estonian thermal power plants and ash plateau sediment from the ash depositories; (2) shale oil processing ash from Petroter type solid heat carrier (SHC) retorts; and (3) shale oil processing ash from Enefit280 type SHC retorts.

The main aims of this thesis are:

- 1) to characterise the effects of different alkaline activator solutions on the polymerization of Estonian oil shale processing residues;
- 2) to study the structural, chemical and mineralogical properties of possible depolymerization-repolymerization reactions and the respective products in alkali activated Estonian oil shale processing residues.
- 3) to characterise the development of cementitious properties and micro-structural characteristics of the alkali activated residues.

The thesis puts forward a central hypothesis that alkali activation of Estonian oil shale processing wastes produces secondary geopolymeric binder phase formation in the material, enhancing its strength and long term durability.

2. ESTONIAN OIL SHALE AND ITS SOLID PROCESSING RESIDUES

Oil shales are sedimentary rocks that contain bituminous organic matter that can be pyrolyzed to extract shale oil and combustible gas or burnt in thermal power plants to produce heat and electricity. Oil shale sedimentary deposits that are both marine or lacustrine in origin are found all over the world, but their industrial scale usage is limited to a few countries including Brazil, China, Israel, Estonia and recently Jordania [16], mainly because of low calorific value of oil shales found in geological record, and different technological and environmental issues. However, ever growing demand for energy resources has created interest in exploiting new oil shale reserves in Green River Formation in USA [17], Huadian and other deposits in China [18], Jordan's oil shale [19], and Queensland deposits in Australia [20].

The Estonian kukersite oil shale is presently the largest industrially used oil shale resource in the world [21]. Estonian oil shale industry has 100 years of experience with large scale oil shale usage [11]. Annual oil shale mining output in recent years has been 18.1–21.5 Mt that covers about two thirds of Estonia's primary fuel balance [22,23]. The majority (ca. 80%) of mined oil shale is utilised in thermal power plants (TPP) for electricity and heat generation, while the rest (19%) is used for retorting shale oil and shale-gas and about 1% is used in cement production [12].

The mineral matter content in oil shale can be as high as 80–90%, but usually is around 40–50%. The main residues from the oil shale industry are ash from electric power production and semi-coke and ash from shale-oil processing into shale oil. At the current production rates, each year 7–8 Mt of ash and nearly 1 Mt of semi-coke are formed in Estonia [23]. With respect to Estonia's population of 1.3 million inhabitants, more than 5 tonnes of solid waste is produced per capita annually.

Oil shale ash has to some extent been used as a constituent in Portland cement, in road construction, for agricultural purposes [24,25], and as a filter material in waste water treatment [26–30]. Nevertheless the secondary usage of ash is only a token (about 2%) of its annual output and reuse is minimal and vast majority of it (ca. 98%) becomes deposited on large ash fields (plateaus) next to power plants. However, higher than average SiO_2 and Al_2O_3 content and lower CaO concentration and L.O.I. values of electrostatic precipitator ash fraction, allow it to be used as an additive in ordinary Portland cement [25,31] that accounts for the majority of the total oil shale ash reuse (ca. 5%). However, all other ash fractions from power plants are not used in any beneficiary way and are hydraulically transported in slurry with a water-to-ash ratio of 20:1 to sedimentation ponds on ash plateaus where it solidifies [13,32]. The ash plateaus occupy an area more than 20 km² and accommodate more than 300 Mt of ash [32].

2.1. Thermal power plant residues

Oil shale is burned in thermal power plants for electricity and heat generation using pulverized firing (PF) or circulating fluidized bed (CFB) combustion technologies with temperatures reaching about 1450 °C and 700–850 °C, respectively [12]. The resultant oil shale ash is a light-colored mineral material that is composed of lime, calcite, anhydrite, different secondary Ca-silicate phases and residual non-carbonate fraction in varying proportions. Composition of the waste depends on processing technology and oil shale feed composition. The remaining ash is Ca-rich with CaO content as high as 55 wt% [13]. Compared to ash wastes from other sources, oil shale ash is, by its composition, most similar to type C fly ash from coal combustion.

The structural, chemical, mineralogical and physical properties of oil shale ash have been thoroughly studied and presented in last decades [13, 31–35]. The cementation of hydrated oil shale ashes is mainly controlled by the formation of stable secondary calcite through slacking of lime and subsequent Ca-hydroxide carbonation, and the formation of Ca-sulfoaluminate hydrate, ettringite, which provides the early strength in the ash systems and also plays an important role in aged materials, though its contribution is diminished [31,36,37].

2.2. Shale oil retorting residues

Oil shale processing into shale-oil and -gas is performed using either Kiviter or solid heat carrier (SHC) process (e.g. Galoter, Petroter or Enefit process) [14,38]. In Kiviter process, hot gas is used as heat carrier, whereas in SHC process hot spent shale formed in the same retorting process is used as a heat carrier. Currently, there are two major SHC technology modifications used for shale oil production in Estonia – Petroter technology is used at the Viru Keemia Grupp and Enefit at Eesti Energia. During retorting the oil shale is heated in the absence of oxygen to a temperature at which its organic part – kerogen – is decomposed or pyrolysed into gas, condensable oil and solid residue, while the inorganic mineral matrix is retained in the form of spent shale.

Shale-oil retorting produces two types of waste depending on the technology used – blackish semi-coke from Kiviter process and dark grey retorting ash (also known as black ash) from Galoter, Petroter and Enefit140 solid heat carrier (SHC) process. A recent modified version of SHC process applied in the Enefit280 technology, leaves a light coloured ash residue similar to that produced in CFB boilers [39].

Semi-coke from Kiviter process is a heterogeneous granular material that is rich in organic residues (up to 10 wt%), including phenols, PAHs (polycyclic aromatic hydrocarbons) and oil products that are potential pollutants with harmful environmental effect [14]. Additional recycled gas and air are admitted to the chambers at the final stage of retorting to burn off the organics from the

residue [40], but due to short residence time the burnout is inefficient. Black ash from Petroter SHC process is however more alike to combustion ash, and contains only a few percent of organics [41,42]. During the SHC process retorting residue is heated up in the presence of oxygen and directed back to the retort chamber. As a result of ash recirculation the burnout is more efficient and the concentration of organics in the ash stays low. Another advantage of SHC technology is that it can use fine grained and unriched oil shale of lower calorific value than the Kiviter process [43].

Physical, chemical and mineralogical properties of black SHC retorting ash have been studied by Talviste et al. [42]. This study shows that black ash contains several reactive phases (e.g. lime, belite) and possesses self-cementitious properties upon hydration. The content of lime (CaO_{free}) in the ash is notably low ($<5 \text{ wt}\%$) and carbonation reactions contribute little to the overall cementation. The black ash however contains considerable amount of cement clinker minerals belite and ferrite which form C-S-H (calcium-silicate-hydrate) gel-like mass providing cementation of the material. Additionally, upon long-term hydration, development of hydrocalumite phase will, to a lesser extent, contribute to the cementation. As a result, the black ash mortars show uniaxial compressive strength values $>6 \text{ MPa}$ after 90 days curing under ambient air conditions [42].

Recently, Eesti Energia AS, the largest Estonian oil shale mining and processing company introduced a new Enefit280 technology, that, by its nature, is an enhanced Enefit140 SHC retorting system, based on Galoter process. Enefit280 retorting unit is combined with CFB combustion boiler where the spent shale and flue gases are combusted at $800 \text{ }^{\circ}\text{C}$ to produce electricity. As a result, the Enefit280 technology is more energy efficient and its overall impact on the environment is reduced, compared to other retorting systems currently in use [39].

The composition of the Enefit280 ash is significantly different from the other retorting residues produced either in the Kiviter type retorts (semi-coke) or other Goloter type SHC retorts including Petroter and Enefit140 (black ash). The ash is grey-beige and does not contain any significant amount of residual organic carbon. In process sequence, pyrolysis residue, which itself recirculates in retort as a heat carrier, is thereafter burnt together with combustible shale-gas in the CFB furnace. This system ensures efficient high temperature conversion of the mineral material in the presence of oxygen. As a result the ash does not contain CaS (oldhamite) and partly oxidised Fe-oxide mineral magnetite [Fe_3O_4 ($\text{FeO}\cdot\text{Fe}_2\text{O}_3$)] that are characteristic to older SHC retorts [14,42], where the waste forms under oxygen deficient conditions. In this sense the ash can be considered to be similar to TPP ashes, particularly to these formed in CFB boilers. However, the content of several reactive phases (e.g. belite-C2S) that are responsible for hydraulic self-cementing, are low in Enefit280 waste heat boiler (WHB) ash (that is the ash from Enefit 280 CFB unit)(Figure 1 in PAPER IV) when compared to other SHC or any other TPP ashes [31,36,37,42]. The ash contains a notably low amount ($<3\%$) of lime (CaO_{free})

and/or portlandite $[\text{Ca}(\text{OH})_2]$ indicating that carbonation reactions do not contribute much to the stabilization of the sediment. Combined with a low content of sulfate, the formation of ettringite upon hydration is subdued in the Enefit280 WHB ash. Ettringite plays an important role in the self-cementing properties of oil shale ash and semi-coke deposits by forming interlocking meshes of needle-like crystals filling the pores space [44]. As a result, the self-cementitious properties of WHB ash are limited upon hydration and compressive uniaxial strength values of $<4\text{MPa}$ are reached after 28 days of curing under ambient conditions (PAPER IV).

3. MATERIALS AND METHODS

3.1. Ash materials

The thermal power plant ash materials were collected from Balti Thermal Power Plant (TPP), Eesti Energia AS (Narva, Estonia). Fresh, unhydrated furnace bottom (BA) and cyclone separator (CA) ash materials were obtained from the ash separation system at a boiler operating on pulverized firing technology. These types of ash were chosen because these are amongst most voluminous ash fractions, which have no secondary use. In addition, hydrated ash plateau sediment (APS) from ash depositories of the same power plant was collected from a 1.5 m deep trench excavated on the ash depository.

The raw, unhydrated ash from SHC type Petroter process (black ash) was collected from Petroter retort ash separation system at Viru Keemia Grupp AS (Kohtla-Järve, Estonia).

Fresh, unhydrated ash from SHC type Enefit280 retort waste heat boiler system (WHB) was provided by Eesti Energia AS (Estonia).

All unhydrated ash materials used in the experiments are, according to the provider, representative of the average ash feed of the specific ash separation unit or system.

3.2. Experimental design and sample preparation

To determine the degree of polymerization reactions upon alkali-activation of the Estonian oil shale industry solid wastes, monolithic test specimens were prepared by mixing the ash materials with the activating solution. As the oil shale solid wastes possesses, upon hydration, cementitious properties the first series of samples were prepared using only deionized water. These samples were used as a reference to determine the degree of polymerization reactions with added alkaline activators. The activating agents used to promote geopolymerization were 5 M sodium hydroxide solution (5M NaOH), commercial sodium silicate (Na_2SiO_3) solution with $\text{SiO}_2/\text{Na}_2\text{O}$ molar ratio of 2.72 and water content of 47.4% (w/w) (hereafter Na-silicate) and a sodium silicate solution modified by sodium hydroxide addition to $\text{SiO}_2/\text{Na}_2\text{O}$ molar ratio 1.5 (hereafter Na-silicate/NaOH) (Table 1 in PAPERS I & II). All sodium silicate based activator solutions were prepared in a way that the added Na_2O to ash ratio in all mix designs was 0.1 (w/w) in order to normalize the amount of added alkali in the mixtures.

All activation solutions were prepared freshly before the mixing. Directly after mixing, the fresh pastes were poured into 40 mm-high and 40 mm-diameter (TPP ash samples) or 23 mm-diameter and 35 mm-high (SHC ash samples) cylindrical moulds and placed on a vibrating plate for 1 minute. The mixing was performed in laboratory environment at an average ambient temperature of 22 °C and relative humidity 50–55%. The samples were then left to cure under the

same conditions in open air ambient environment for 7 and 28 days in experiment using TPP ashes and for 7, 28 and 90 days for SHC ash mixtures. The water binding capacity of each type of material derived under pore space saturation conditions were determined experimentally before preparation of mixtures and the corresponding ratios were used in the mix design to ensure full reactivity and maximal dissolution of the silicate and aluminosilicate phases present in the solid wastes.

3.3. Analytical methods

The uniaxial compressive strength of the materials as an initial indicator of the degree of polymerization reactions was measured under continuous loading ($20 \text{ kPa} \cdot \text{s}^{-1}$) until specimen failure. Compressive strength was measured in three replicas after 7 and 28 days of curing for TPP and WHB ash mixtures and after 7, 28 and 90 days of curing for SHC black ash mixtures.

Chemical composition of the ash materials was determined by means of X-ray fluorescence spectrometry (XRF) on Rigaku Primus II XRF spectrometer using SQX quantification model standardised against in-house ash sediment standard materials.

Mineral composition of the test samples and original ash materials was determined using X-ray diffraction (XRD) analysis. Prior to the XRD and XRF analyses, the materials were dried at 105°C for 2 hours. Ground and homogenized randomly oriented powder samples were measured on a Bruker D8 diffractometer using Ni-filtered $\text{CuK}\alpha$ radiation and LynxEye linear detector over the $2\text{--}70^\circ 2\theta$ region. Mineral composition of the samples was interpreted and modelled using Rietveld algorithm based code Topaz 4.0. To determine the quantity of the amorphous glassy phase that is not detected by the conventional XRD method, the SHC ash test specimens were spiked with 10 wt% of ZnO prior to XRD measurement. The amorphous phase in the material absorbs X-rays and causes an apparent lower ZnO content than the sample was spike with. The amorphous phase content was calculated based on the difference between the added and measured spike phase concentration. Aluminosilicate composition was assumed for the glass phase.

The thermogravimetric (TGA) and differential thermal analysis (DTA) of raw TPP ash materials was performed on STA 449 F3 Jupiter thermal analyzer in Al_2O_3 crucibles by heating to 1000°C at $10^\circ\text{C min}^{-1}$. Total organic carbon (C_{org}) in the original fresh black ash was measured as the loss on ignition at 550°C for 2 hours, and total loss on ignition (L.O.I.) of all samples was measured at 950°C for 2 hours.

The microstructure and chemical composition of fresh unhydrated ashes and test monoliths were investigated using Zeiss EVO15MA scanning electron microscope (SEM) with Oxford X-MAX energy dispersive detector and AZTEC X-ray analytical system. Samples were analysed both uncoated in the variable pressure mode and coated with gold or platinum in the high vacuum mode.

Attenuated Total Reflectance – Fourier transform infrared spectroscopy (ATR-FT-IR) patterns were measured using a “Smart Orbit” diamond ATR-accessory attached to Thermo Scientific Nicolet 6700 FT-IR spectrometer with CsI optics and DLaTGS detector at the Institute of Chemistry, Tartu University. Transmittance IR spectra were collected from 225–4000 cm^{-1} at a resolution of 4 cm^{-1} with 128 scans per sample.

Solid state ^{29}Si MAS-NMR (magic angle spinning nuclear magnetic resonance) measurements from source material and ground samples after 28 (CA and SHC black ash) and 90 (SHC black ash) days of curing were conducted at the National Institute of Chemical Physics and Biophysics (Tallinn, Estonia), on a Bruker AVANCE-II nuclear magnetic resonance (NMR) spectrometer attached to a 8.5 T magnet (^{29}Si resonance frequency 71.4 MHz). About 1.5g of each sample was rotated at 5 kHz in 10 mm zirconia rotors using home-built MAS probe. The spectra were recorded with single-pulse excitation with a relaxation delay of 100 s. Number of scans was 800 to 1600. The chemical shifts are given relative to tetramethylsilane (TMS) reference.

4. RESULTS AND DISCUSSION

4.1. Thermal power plant residues

4.1.1. Phase composition and microstructure

Fresh, unhydrated, BA and CA ash from Balti thermal power plant contain lime, portlandite, anhydrite, calcite, quartz and secondary Ca-silicates. Most abundant reactive Ca-phases in TPP ash are belite/C2S (β - Ca_2SiO_4) and lime (CaO_{free}) (Table 3 & Figure 1 in PAPER I). The deposited ash is subjected to mineral alteration upon hydration and the stabilized ash plateau sediment (APS) is composed of Ca-carbonate (calcite and vaterite), ettringite, bassanite, gypsum and Ca-silicates (Figure 2 in PAPER I). The DGA/DTA analyses of raw TPP ashes and APS (Figure 3 in PAPER I) agree with the XRD data. Thermal effects corresponding to portlandite and calcium carbonates were distinguished in all of the materials and evaporation of free water and the loss of water molecules upon dehydration of hydrous phases such as gypsum, ettringite and possibly a C–S–H phase was additionally distinguished in APS.

The X-ray diffraction patterns of BA and CA ash mixtures prepared with water and 5M NaOH show the dissolution of reactive and water soluble phases, and the formation of portlandite [$\text{Ca}(\text{OH})_2$], that is a product of CaO_{free} (lime) hydration (Figure 1 in PAPER I). However, XRD patterns of ash mixtures activated with solutions containing soluble silicate also reveal formation of an amorphous calcium-silicate-hydrate phase (C–S–H gel) that is indicated by a diffuse maxima in $30^\circ 2\theta$ $\text{CuK}\alpha$ region. This maxima is however absent in 5M NaOH treated ash mixtures, indicating that there is no, at least substantial, formation of secondary amorphous silicate binder phases. Thus, NaOH activation of the oil shale ash at ambient conditions does not lead to sufficient dissolution of the material and the formation of crystalline zeolites, opposed to the case of NaOH activation at higher temperatures [45,46] (PAPER I). From the relative intensities of portlandite peaks it is apparent that silicate availability is the limiting factor for C–S–H phase formation, as excess Ca is precipitated in the alkaline medium as portlandite. In contrast to unhydrated ash mixtures, the XRD patterns of mixtures with APS material show only dissolution of reactive and water soluble phases without the formation of any new crystalline or amorphous phases (Figure 1 in PAPER I).

SEM imaging of hydrated and 5M NaOH activated TTP ash samples revealed similar matrix structure showing glassy spherules in different states of dissolution and secondary calcium carbonate and portlandite crystal aggregates (Figure 7 in PAPER I). However, mixtures activated with Na_2SiO_3 based solutions show predominant amorphous calcium silicate matrix that occasionally encompasses unreacted or semi-reacted glass spherules and unreacted portlandite and is cut with fracture networks. According to SEM-EDS analysis the average composition of this amorphous matrix is Ca 23.2 wt%, Si 15.9 wt%, Na 6.6 wt%, Al 1.0 wt% that is similar to non-stoichiometric composition of a

C-(A)-S-H (calcium-aluminium-silicate-hydrate) gel. This matrix evidently results from reactions between soluble sodium silicate and dissolved calcium from the reactive phases in the ash material (PAPER I).

4.1.2. Structural characteristics of geopolymerization

ATR-FT-IR spectra of all activated TPP ashes and APS samples were collected after 7 and 28 days (Figures 4 & 5 in PAPER I). All spectra are characterised by bands due to C-O vibrations in carbonates, with band around 1410–1430 cm^{-1} representing C-O in-plane bend in CO_3^{2-} ion, 873 cm^{-1} corresponding to C-O out-of-plane bend and 712 cm^{-1} C-O in-plane bend in CO_3^{2-} ion with the latter two corresponding to ν_2 and ν_4 bending vibrations in calcite [47,48]. The broad vibration band in activated TPP ashes centred around 3300–3400 cm^{-1} along with the band at 1645 cm^{-1} represent O-H stretching and bending vibrations in water molecule and the vibration band at 3640 cm^{-1} corresponds to O-H vibration in portlandite [$\text{Ca}(\text{OH})_2$]. All samples also show a group of bands corresponding to symmetric and asymmetric stretching and bending vibrations of Si-O and Si-O-(Si/Al) bonds in silicate mineral phases that appear between 400–1200 cm^{-1} . Vibration band of Si-O bonds at 1110 cm^{-1} and the band around 440 cm^{-1} that is due to deformation of SiO_4 tetrahedra [49] are attributed to different silicate phases present in the ashes. The spectra of APS based samples do not show any changes in main peak positions between different sampling times and mixtures, indicating that no significant structural changes have occurred in the activated APS materials (Figure 5 in PAPER I).

BA and CA ash based samples activated with alkaline solution, however, exhibit a variety of changes in the Si-O-(Si/Al) vibration ranges. A shift of the main Si-O vibration band at 970 cm^{-1} to lower wavenumber [49] and appearance of the Si-O ν_2 bending vibration band at 485 cm^{-1} [50], indicate depolymerization of the initial silicate structures (PAPER I).

In samples activated using sodium silicate containing solutions the band at 670 cm^{-1} corresponds to Si-O-Si stretching vibrations of SiO_4 tetrahedra in C-S-H and changes in 670–600 cm^{-1} region correspond to Si-O-(Si) vibrations, indicate restructuring of the SiO_4 tetrahedra [50]. The vibration band at 811 cm^{-1} corresponds to Si-O stretching of SiO_4 tetrahedra in C-S-H gel, corresponding to Q^1 chain end-group configuration [49]. The position of the main Si-O band at around 930 cm^{-1} indicates that the hydrate gel phase is mainly composed of silica tetrahedron in Q^1 and Q^2 , $Q^2(1\text{Al})$ configuration, corresponding to a C-S-H type phase [51] (PAPER I). The silica tetrahedron in silicates can have up to four nearest neighbour silica tetrahedra connected via oxygen bridges. In commonly used $Q^n(m\text{Al})$ notation n indicates the number of connected nearest neighbours and m indicates the number of neighbouring AlO_4^- ions, that have been substituted into the silicate framework in place of SiO_4 . Thus, Q^0 denotes monomeric orthosilicate anion SiO_4^{4-} , Q^1 the end-groups of chains or paired units (disilicates), Q^2 middle groups of chains or

cycles, Q^3 chain branching sites and Q^4 three-dimensionally cross-linked groups.

Formation of a C–S–H phase in the activated ash mixtures was further confirmed by ^{29}Si MAS-NMR spectra in mixtures with cyclone ash. The spectrum of initial unhydrated cyclone ash (Figure 6 in PAPER I) shows resonances at -71.7 ppm that corresponds to Q^0 Si in belite, a weaker line at -73.8 ppm overlapping with belite that belongs to Si in alite (Q^0 , C3S phase) and a very weak resonance line at -108.4 ppm that is characteristic to Q^4 configuration of Si in quartz (SiO_2) [52]. Wide modelled maxima at about -80 and -100 ppm correspond to the different silicon sites in amorphous glass phase [45].

NMR spectra of the ash activated with sodium silicate based solutions (Figure 6 in PAPER I) show complete dissolution of quartz and glass phase. Line at -78.5 ppm in those spectra indicates Si in Q^1 configuration, the presence of silica chain ends and paired units; line at -84.4 ppm shows Q^2 configuration, formation of chains of SiO_4^{4-} anions; the line at -81.3 ppm corresponds to Si in $Q^2(1\text{Al})$ configuration (one of the Si neighbours in Q^2 formation is replaced by Al) and are characteristic to silicon sites in C–S–H [52,53]. Aluminium substitution into the silicate structure, denoted by $Q^2(1\text{Al})$ unit, indicates that the gels are of a C–(A)–S–H, rather than a simple C–S–H type (PAPER I). As far as Al is assumed to be confined to the “bridging” sites of dreierkette-based silicate chains, then its incorporation can lengthen the chain structure [54]. The broad Lorentzian line centred at 72 ppm, attributed to Q^0 site in anhydrous silicates, indicates the formation of another unidentified binder alongside C–(A)–S–H gel [55–58]. Weak lines at -71.67 ppm and -73.8 ppm indicate that some amount of Ca-silicate phases (belite/alite) have preserved the activation.

The wide maxima at about -85 ppm in spectra of hydrated and 5M NaOH activated ash, corresponding to primary amorphous glass, indicates that the activating solution was not sufficient in fully dissolving and depolymerizing the initial silicate structures (PAPER I). However, the spectra of 5M NaOH activated ash exhibits lines at -78.4 ppm, -81.5 ppm and -83.8 ppm corresponding to Q^1 , $Q^2(1\text{Al})$ and Q^2 silicon sites in C–(A)–S–H, respectively [52,53].

Also, the Ca/Si ratio of C–S–H has been shown to be linked to the structure of the gel [59–63]. The high Ca/Si ratio of 1.46 found in SEM-EDS analyses of the gel-like matrix in studied samples (PAPER I) corresponds well with ^{29}Si MAS-NMR and ATR-FT-IR results whereas it has been earlier noted that Ca/Si ratio >1 results in depolymerization of the C–S–H structure [49,50]. Furthermore, this implies that the structure of this material is mainly one-dimensional [61].

4.1.3. Strength development

Thermal power plant ashes and APS activated with 5M NaOH do not show any significant increase in compressive strength compared to water-based mixtures and the values do not exceed 1.3 MPa (Figure 8 in PAPER I). Compressive strengths of samples activated with solutions containing Na_2SiO_3 were much higher with CA and BA ash based samples reaching >8 MPa whereas samples activated using lower $\text{SiO}_2/\text{Na}_2\text{O}$ ratio of 1.5 exhibited greater and more uniform strength gain (Figure 8 in PAPER I).

However, mixtures of ash plateau sediment with solutions containing soluble silica did not show any increase in strength. Fairly similar compressive strengths (6.5–8.3 MPa) after 7 and 28 days were obtained for bottom and cyclone ash samples with Na-silicate/NaOH activation. Nevertheless, in mixtures with Na-silicate, the cyclone ash samples show a more than two-fold increase in compressive strength after 28 days (7.5 MPa) if compared to sample tested after 7 days (2.8 MPa) that indicates continuing dissolution of Si (and Al) from amorphous glass phase and Ca-silicate mineral phases and polymer formation. However, a significantly lower value of the compressive strength for lime (CaO_{free}) rich bottom ash mixtures with soluble silica after 28 days (0.7 MPa) compared with the test after 7 days (3.2 MPa) are probably due to flash setting of the mixture, which can be caused by fast reactions between Ca ions released by dissolution of free lime and the Na_2SiO_3 . As a result, the activator was consumed at early stages of curing and the polycondensation giving the strength is not developed.

4.2. Petroter type solid heat carrier shale oil pyrolysis residues

4.2.1. Phase composition and microstructure

The average mineral composition of the crystalline phases and an amorphous phase of fresh SHC black ash is dominated by calcite, quartz and K-feldspar, and some dolomite is also present (Table 2 in PAPER II). All of these components are also characteristic of raw oil shale. In addition, black ash contains secondary phases formed during thermal treatment of oil shale: authigenic Ca silicates, periclase, free lime and oldhamite. Oldhamite is a CaS phase that is particularly characteristic of black ash and does not occur in TPP ashes that are the by-products of oil shale thermal combustion. Oldhamite forms under oxygen deficiency conditions in the reaction between CaO and H_2S . Another mineral indicating oxygen deficiency during black ash formation is the partly oxidized Fe-oxide mineral magnetite [Fe_3O_4 ($\text{FeO} \cdot \text{Fe}_2\text{O}_3$)], while in the TPP ashes, hematite Fe_2O_3 is typically present. In addition, a dehydrated mica-like clay phase was identified in black ash. The content of the amorphous aluminosilicate glass phase varies in fresh black ash from 3.0 to 7.2 wt%, and the average content of the amorphous phase is 5.7 wt% (Table 2 in PAPER II).

The chemical composition of the fresh black ash (Table 3 in PAPER II) corresponds to the mineral composition of the samples studied and is dominated by CaO and SiO₂ that compose on average 32 wt% and 21 wt%, respectively. The content of MgO, Al₂O₃ and Fe₂O₃ in fresh ash is on average less than 10 wt%, and the sulfur content is 2 wt% on average. The carbon content (C_{total}) is approximately 7 wt%, and the content of organic carbon (C_{org}) is 1.5–2.2 wt%.

X-ray diffraction analysis of black ash mixtures show that characteristic phases in mixtures prepared with plain water are secondary ettringite and hydrocalumite that form upon hydration of the ash (Figure 1 in PAPER II). Also portlandite, formed by CaO_{free}(lime) hydration, appears after 7 days. After 28 and 90 days, the changes in the mineral composition of the water-hydrated black ash samples compared to the composition of the mixture after 7 days are rather small (Table 2 in PAPER II). Only portlandite has practically disappeared, and the relative content of calcite has increased, which is evidently due to portlandite carbonation. There is also a slight increase in ettringite content up to 7.6 wt%, and the amorphous phase is practically absent, as it is less than 1 wt% after 28 and 90 days.

Evolution of the mineral composition in samples treated with 5M NaOH activator is similar to the changes in the samples mixed with plain water (PAPER II). The content of the dominant secondary phases formed in samples treated with NaOH differ compared with water-treated samples (typically ±5 wt%). However, there are a few specific differences between water-mixed and NaOH activated samples. The most important difference compared to the samples treated with water is the absence of ettringite in the NaOH activated mixture. Additionally, the content of hydrocalumite is approximately 4 wt% higher in the 7-day samples and 5 to 7 wt% higher in the 28- and 90-day samples than in specimens mixed with water and portlandite is present even after 90 days. Moreover, the authigenic clay mineral identified as smectite (montmorillonite) appears in low content (0.5 wt%) after 7 days of hydration and has a slightly higher content (2.1 wt%) after 90 days (Table 2 in PAPER II). There is also an increase in the amorphous phase after 90 days, which could indicate the formation of an amorphous geopolymer phase. However, the relative error in amorphous phase measurements can be as high as 30 to 50% and its estimate must be considered with caution. Nevertheless, the formation of authigenic smectite clay in this mixture indicates dissolution and recrystallization of Si and Al phases, which supports the observed increase in the amorphous phase.

In contrast to water and NaOH mixtures there is no secondary ettringite and/or hydrocalumite phases present or other noticeable changes in phase composition of crystalline phases (except dissolution of CaO_{free} and CaS phase) in neither Na-silicate and Na-silicate/NaOH activated ash samples at any stages of curing (Figures 3 & 4 in PAPER II). A distinct and major change compared to fresh black ash samples and water- and NaOH-mixed samples is the increased content of the amorphous phase (Table 2 in PAPER II). This change

is due to the formation of amorphous Ca-Na-Al-silicate gel from the reaction between Na-silicate solution and the minerals present in black ash (PAPER II). However, there are no significant mineralogical differences between samples activated by Na-silicate and samples treated with Na-silicate/NaOH solutions. Differences in mineralogical composition in these two different mixtures vary over the range of a few percent (Table 2 in PAPER II), indicating similar changes in both mixtures. For chemical composition, the observed changes in Na-silicate and Na-silicate/NaOH mixtures compared with original fresh ash are related to the addition of Na and Si. In the samples prepared with sodium silicate based activators, the SiO_2 content has increased to 32.5 wt% in the sample prepared with Na-silicate/NaOH and to 38 wt% in the sample prepared with only Na-silicate (Table 2 in PAPER II).

Scanning electron microscopy (SEM) analysis of the original black ash shows that the material is fine-grained with particle size generally less than 60 μm , and the material is dominated by fine particles with diameter <20 μm (Figure 5a, b in PAPER II). The particles are irregular in shape, and the finest particles are somewhat aggregated into lumps approximately 20–30 μm in size. Samples mixed with water show intensive cementation and development of secondary Ca-Al and Ca-Al-sulfate minerals in the material pore space (Figure 5c, d in PAPER II). The ash particles are covered by secondary precipitates, and bonds between particles are generated by interlocking needle- and lath-shape authigenic minerals that can be identified by crystallite morphology and chemical composition as hydrocalumite, ettringite and secondary calcite (PAPER II).

Mixtures activated with NaOH solution show a microstructure similar to water-mixed samples, but ettringite is not identified and the pore-space is filled with hydrocalumite platy crystals and crystal aggregates (Figure 5e, f in PAPER II). This finding agrees well with the mineralogical analysis showing the absence of ettringite and the presence of abundant hydrocalumite in the ash-NaOH system. The microstructure of Na-silicate/NaOH and Na-silicate activated mixtures is considerably different from the water and NaOH mixtures and similar to each other (Figure 6 in PAPER II). SEM images show that the solidified material is filled in by amorphous glassy-like masses. SEM-EDS analysis of the gel-like matrix, filling the area between unreacted ash particles, shows that it is a (Na)-Ca-Al-Si hydrate with Na/Ca/Al/Si ratio of about 18/32/7/43 (Figure 5 in PAPER III). This amorphous matrix is strongly fractured, and practically all surfaces are cut with dense fracture networks. Fracturing already occurs in samples after 7 days of curing but is specifically intense in samples analysed after 90 days. However, the development of cracks can also be due to dewatering of the gel under vacuum conditions in the electron microscope, but the same pattern was observed both under high and low vacuum conditions, indicating that the fracturing is not induced solely by the vacuum but also by the recrystallization and dewatering of the polymerized gel during the curing.

4.2.2. Structural characterization of geopolymerization processes in SHC black ash mixtures

ATR-FT-IR spectra of initial ash, and different activated SHC ash mixtures after 7, 28 and 90 days are characterized by the well-defined/sharp bands at 1400 cm^{-1} , 870 cm^{-1} and 712 cm^{-1} representing C–O stretch and bend of CO_3^{2-} ion, in carbonates [47,48]. The shoulder at 1120 cm^{-1} and low-intensity band at 594 cm^{-1} in the original ash spectrum correspond to the stretching and bending of S–O bond in SO_4^{2-} ion in anhydrite, respectively [48] which is also in correlation with mineralogical composition.

Several important changes in the ATR-FT-IR spectra of activated samples compared with original ash are evident in all sample series. First of all, new bands around $3300\text{--}3400\text{ cm}^{-1}$ and 1640 cm^{-1} , representing O–H stretching and bending vibrations in water molecule appear in all mixtures. The ATR-FT-IR spectra of ash treated with plain water (Figure 3a in PAPER III) show a band around 970 cm^{-1} associated with Si–O(–Si/Al) vibrations [49]. This band shifts in water-ash mixtures to higher wavenumbers after 7 days and then shifts back to lower wavenumbers after 28 and 90 days of curing, indicating that initially formed structures deform in time. The broad band at 1110 cm^{-1} is a combination of Si–O stretching vibrations from amorphous silicate phases associated with Q^3 silicon sites [64] and S–O vibrations in SO_4^{2-} , arising from different sulfate minerals like gypsum and ettringite. As the XRD patterns of the water-ash mixtures also show presence of ettringite (PAPER II) then it is not clear if the band at 1110 cm^{-1} could be associated with the dissolution and depolymerization of the amorphous glass phase and its subsequent polymerization as branching Q^3 silicon species.

ATR-FT-IR spectra of NaOH activated ash mixtures (Figure 3b in PAPER III) show that a notably sharp band at 3640 cm^{-1} is present, characteristic to O–H stretching in portlandite $[\text{Ca}(\text{OH})_2]$ [65]. The Si–O(–Si/Al) asymmetric stretching vibrations band in these mixtures is split into two components, at around 950 cm^{-1} and around 990 cm^{-1} that can be associated with Si–O–Al and Si–O–Si stretching vibrations in $\text{Q}^2(1\text{Al})$ and Q^2 silicon site respectively [51]. The increase in the intensity of the 990 cm^{-1} band after 28 days shows that the relative abundance of Q^2 silicon sites has increased. Similar to water-ash mixture the band at 1117 cm^{-1} in NaOH activated mixture after 7 days of curing can be attributed to S–O stretching vibrations in Ca-sulfate phase [48] although neither gypsum nor ettringite was detected in XRD analysis of these samples. Alternatively, this band can be attributed to the Si–O vibrations in amorphous silicate phases though the band at 670 cm^{-1} , not present in other mixtures, also indicates of S–O bending vibrations in gypsum. Nevertheless, the ATR-FT-IR spectrum of the NaOH activated sample after 90 days indicates a shift of the 1117 cm^{-1} band to a higher frequency of 1126 cm^{-1} (Figure 3b in PAPER III) that can be associated with the polycondensation of the silicon species in the amorphous phase.

The ATR-FT-IR spectra of initial black ash and samples prepared using sodium silicate solution (Figure 3c, d in PAPER III) show a Si–O(–Si/Al) stretching band around 960 cm^{-1} corresponding to Q^2 silicon site. This band shifts to lower wavenumbers (959 cm^{-1}) from the initial position in original ash (963 cm^{-1}) after 7 days which indicates that during alkali activation, bridging oxygen atoms in initial aluminosilicate are replaced by two non-bridging oxygen atoms with a negative charge and that Al is being substituted into the silicate network [66]. Through that process the TO_4 ($T = \text{Si or Al}$) tetrahedrons within the network have become more isolated and, consequently, the T–O bonds should possess lower molecular vibration force constants, resulting in shift of the infrared band to smaller wavenumbers [67]. This initial shift to lower wavenumbers also corresponds to the previous studies [64], showing that higher Na^+ content leads to the Si–O band shifting to lower wavenumbers. After 28 and 90 days it appears that this band shifts progressively to higher wavenumbers from initial 959 cm^{-1} after 7 days to 962 cm^{-1} and to 979 cm^{-1} after 28 and 90 days, respectively, which suggests that the material continues polymerization and polymer chains are becoming longer through incorporation of more tetrahedra in Q^2 chain mid-member position [49].

ATR-FT-IR spectra of the ash activated with Na-silicate/NaOH solution show a similar shift of the Si–O(–Si/Al) band to lower wavenumbers at the beginning and later shift to greater wavenumbers, indicating to the same tendency of depolymerization and polymerization as observed in the Na-silicate activated samples (Figure 3d PAPER III).

The NMR spectra of initial black ash (Figure 4 in PAPER III) shows a broad maxima in the range from -80 to -105 ppm , which can be attributed to the different silicon sites in amorphous glass phase [45]. In addition, there is a resonance line at -72.7 ppm that arises from Q^0 sites in secondary Ca-silicate phases belite and alite [68] whereas the peak at -108.1 ppm can be assigned to Q^4 site in quartz [52]. Most of the ^{29}Si MAS-NMR peaks in ash-water mixtures after 28 days of curing are comparable to initial ash spectrum. The intensity of belite/alite peak has decreased, but the peak attributed to quartz shows no change. However, new resonance lines at -79.9 , -85.2 , -95.4 and -100.9 ppm appear in hydrated ash and can be attributed to Q^1 , Q^2 [55–57,69], silicon sites, and an amorphous phase dominated by Q^3 [1] silicon sites, respectively. The changes in the spectrum measured after 90 days of curing suggest that initially formed silicate structures have disintegrated and the spectrum has taken a shape comparable to the spectrum of initial ash. The peaks of Q^1 and Q^2 silicon sites are still present at -82.5 and -86.2 ppm but their intensities have decreased. A new major resonance line centred at -91.6 ppm has appeared which is similar to a maximum in the original ash spectrum and can be attributed to different silicon sites in amorphous glass (PAPER III).

The ^{29}Si MAS-NMR spectra of NaOH activated black ash samples (Figure 4 in PAPER III) show notable differences compared with original ash and the ash-water mixtures. After 28 days of curing the relative intensity of the belite/alite peak has decreased and the different silicon sites attributed to

amorphous glass phase are no longer present or have considerably decreased in intensity. The spectra show resonance lines at -78.9 ; -81.7 ; -84.0 and -100.8 ppm which arise from the silicon sites Q^1 , $Q^2(1Al)$, Q^2 and Q^3 [52], respectively. The broad resonance line at -96.5 ppm could be associated with amorphous silicate phase which remains after the alkaline treatment of the ash and the peak at -108.0 ppm belongs to quartz. This indicates that most of the initial glass phase has dissolved, and a new silicate chain-structure has formed. The presence of $Q^2(1Al)$ site in the middle group of a silicate chain indicates Al-substitution in the structure. After 90 days the relative intensity of the peak corresponding to Q^1 silicon site has decreased, but at the same time the relative intensity of the peaks attributed to Q^2 sites show increase, meaning that there are more Si–O–Si–O–Si middle groups and the length of the silicate structures has increased. This suggests continuing polymerization and growth in silicate chain length in black ash mixtures with NaOH. However, the presence of the amorphous phase arising from the hydration of the glass and primary silicate phases even after 90 days reveals that 5M NaOH solution was not sufficient to dissolve all the silicate phases present in the source material

NMR spectra of the ash activated with Na-silicate (Figure 4 in PAPER III) show major changes compared with original ash and ash-water mixtures, and the NaOH activated mixture (PAPER III). The peak respective to belite/alite has completely disappeared, the peak of quartz at -108.4 has decreased and one new broad intensive peak centred approximately at -89 ppm along with a smaller peak at around -108.7 , which can be assigned to cross-linking Q^4 silicon site, have appeared in the spectra. This broad peak is characteristic in Na-silicate activated systems that has been interpreted to originate from the chain mid-member Q^2 groups [1]. It bears resonance characteristic similar to semi-crystalline C–S–H gel, however, the C–S–H gel in the Na-silicate activated sample is different of the binding C–S–H gel-phase present in Portland cement which has the peaks centred at -80 and -86 ppm [51,55], with the more negative chemical shift pointing to a presence of longer aluminosilicate chains [51]. In ordinary Portland cement the resonance peaks are assigned to Q^1 end groups and Q^2 middle groups, suggesting that the silicate groups are organized in shorter linear finite chains [70]. Additionally, the broad peak centred at -89 ppm could correspond to chain branching sites (Q^3 units) and three-dimensional cross-linked sites (Q^4 units), both with substantial Al substitution for Si as an indicative of a polymerized structural aluminosilicate framework of a geopolymeric phase [55,56,71]. This indicates that the polymerized structure, rather than being a simple C–S–H chain structure, is of cross-linked aluminium substituted C–(A)–S–H type (PAPER III).

Comparison of the NMR spectra of Na-silicate activated mixtures after 28 and 90 days shows that the main peak has shifted slightly towards more negative chemical shift values and the broad Q^4 silicon band has increased in intensity (Figure 4 in PAPER III). This is an indication of continuing polymerization process where the aluminosilicate chains are rearranging and

growing in length, which is in accordance with the observations from ATR-FT-IR.

The ^{29}Si MAS-NMR spectra of ash mixtures activated with Na-silicate/NaOH solution (Figure 4 in PAPER III) show a combination of features observed with NaOH and Na-silicate activation. Resonances corresponding to belite/alite and quartz are present but, compared with original ash, of significantly lower intensity. The spectra, similar to NaOH mixtures, show new resonance peaks at -79.2 , -82.3 and -85.5 ppm assigned to Q^1 ; $\text{Q}^2(1\text{Al})$ and Q^2 respectively. The broad C-(A)-S-H gel peak is centred at -92.5 ppm indicating to Q^3 branching silicate units. Notably, the intensity of the C-(A)-S-H peak has increased after 90 days of curing suggesting ongoing polymerization of aluminosilicate species, as more tetrahedral units are incorporated into the structure.

4.2.3. Strength development

Compressive strength of hydrated black ash show a steady growth over the curing period, reaching on average 2, 6 and 8 MPa after 7, 28 and 90 days of curing, respectively (Figure 7a in PAPER II). In samples activated with 5M NaOH the compressive strength stays low (< 1.7 MPa) after 7 and 28 days of curing and the compression curves are characterized by high residual strength (Figure 7b in PAPER II, Figure 1 in PAPER III). Cementation and peak strength (up to 4.3 MPa) are developed only after 90 days of curing and furthermore indicate the formation of an amorphous silicate binder and polymerization of silicate species, indicated by XRD, ATR-FT-IR and ^{29}Si MAS-NMR results.

Na-silicate and Na-silicate/NaOH activated samples show remarkably different behaviour compared to samples hydrated with water and activated with NaOH (Figure 7c, d in PAPER II, Figure 1 in PAPER III). Both mixtures show high strength values after 7 days reaching up to 10.4 MPa in Na-silicate activated ash, and 7.75 MPa in Na-silicate/NaOH, respectively. However, in the second case the values did not change much with extended curing time, and in the first case the values dropped significantly after curing for 28 days with practically the same uniaxial compressive strength after 90 days as in 28th day (Figure 7c, d PAPER II). Both materials show characteristic brittle behaviour, but the break-down of the sample occurs at significantly lower loadings after 28 and 90 days. This drop in compressive strength in Na-silicate and Na-silicate/NaOH activated samples was accompanied by a significant reduction in sample sizes (measured as the diameter and length of the tested cylinders) already after 7 days of curing, and the diameter and length of the samples decreased up to 10% and 5% after 90 days of curing, in Na-silicate and Na-silicate/NaOH activated samples, respectively.

4.3. Enefit280 type solid heat carrier shale oil pyrolysis residues

4.3.1. Phase composition and microstructure

The mineral composition of the crystalline phases and an amorphous phase of the fresh Enefit280 waste heat boiler (WHB) ash (Figure 1 in PAPER IV) is dominated by calcite (44.5 wt%), quartz (8.1 wt%) and K-feldspar (7.7 wt%) with some dolomite (1%), representing the inherited sedimentary mineral phases that are characteristic to raw oil shale. In addition, the WHB ash contains secondary phases formed during the thermal treatment of oil shale – authigenic Ca-silicates (11.2 wt%) and periclase (1.0 wt%), but it is notably low (<2 wt%) in lime (CaO_{free}). The level of the amorphous phase in the fresh ash is about 14 wt% (PAPER IV). The chemical composition of the fresh WHB ash corresponds to its mineral composition and is dominated by SiO_2 and CaO that on average make up 25.5 wt% and 30.22 wt%, respectively (Table 1 in PAPER IV). The level of MgO , Al_2O_3 and Fe_2O_3 in the fresh ash is on average 1.95, 11.13 and 4.83 wt%, respectively. The content of SO_3 varies between 1.5–4.2 wt% with an average of 3.97 wt% (PAPER IV). Variation in the chemical composition of the test samples arise from the additional Si and Na in the activator solution and carbonation reactions indicated by higher L.O.I. values (Table 1 in PAPER IV).

Changes in the mineral composition of the hydrated samples are characterized by disappearance of lime CaO_{free} and portlandite [$\text{Ca}(\text{OH})_2$] phase, as well as the formation of a secondary Ca-Al hydrate phase hydrocalumite and a hydrous Ca-Al-sulfate phase ettringite (Figure 1 in PAPER IV). The formation of these secondary phases is accompanied by a drop in the amorphous content after 7 days of curing. This might indicate that some part of the X-ray amorphous phase was dissolved and recrystallized into a crystalline phase, in this case hydrocalumite and ettringite. However, after 28 days the hydrocalumite has practically disappeared and the relative content of the amorphous phase shows an increase, indicating that the metastable phases including the Ca-silicate phases and hydrocalumite have started to decompose, possibly forming a (semi)-amorphous C–S–H phase (PAPER IV).

The evolution of the mineral composition in the samples treated with the NaOH activator shows marked differences with samples hydrated with plain water. In NaOH activated mixtures hydrocalumite and portlandite were present in the samples throughout the curing period whereas the presence of ettringite was not detected (Figure 1 in PAPER IV). Changes in the chemical composition, between the fresh ash and 28-day-old NaOH-water mixtures are exemplified by the increase of Na_2O in the latter, which is due to the addition of NaOH and increase in the L.O.I. values, which is possibly due to the carbonation of portlandite.

The mineral composition of the WHB ash specimens made of mixtures with sodium silicate based solutions differ considerably from the samples treated

with water or NaOH (PAPER IV). A distinct and major change is denoted by the content of the amorphous phase, which varied from 6 wt% to 52 wt% in the samples mixed with Na-silicate. This is evidently due to recrystallization reactions and most importantly the formation of amorphous Ca-(Na)-Al-silicate gel in the reaction between the Na-silicate solution and the minerals present in the WHB ash (PAPER IV). No significant mineralogical differences were discernible between samples activated by Na-silicate and Na-silicate/NaOH solutions, indicating similar changes in both mixtures. The observed changes in the chemical composition of the Na-silicate and Na-silicate/NaOH mixtures, when compared to the original fresh ash, are related to the addition of Na and Si (Table 1 in PAPER IV).

The SEM analysis of the original WHB ash shows that the material is fine grained with a particle size generally less than 100 μm and that the material is dominated by fine particles with a diameter of $\sim 20\ \mu\text{m}$ (Figure 3a in PAPER IV). The particles are irregular in shape and the finest particles are somewhat aggregated into lumps of 20–30 μm in size (Figure 3b in PAPER IV). The microstructure of hydrated samples (Figure 3c in PAPER IV) shows recrystallization and development of secondary precipitates and the bonds between particles are generated by interlocking needle and lath-shape authigenic minerals. Their crystallite morphology and chemical composition identifies them as hydrocalumite and ettringite, even though the relative abundance and particularly the size of the lath-needle-like ettringite crystallites is much smaller than that observed in other hydrated oil shale ashes [32] (PAPER IV).

NaOH activated mixtures show a similar microstructure to hydrated samples (Figure 3d in PAPER IV), but their pore-space is filled with hydrocalumite platy crystals and crystal aggregates while no lath-shape ettringite crystals are detected. The microstructure of the Na-silicate/NaOH and the Na-silicate activated mixtures is considerably different from the water and NaOH beased mixtures and are similar to each other (Figure 3e, f in PAPER IV). Under SEM the energy dispersive analysis of the material shows that it is composed of a Ca-Na-Al-silicate gel-like matrix that is completely filling the area between the unreacted ash particles but is strongly fractured. This agrees with the higher amount of the amorphous phase revealed in the XRD analysis of these mixtures.

4.3.2. Structural characterization of geopolymerization processes in SHC WHB ash mixtures

ATR-FT-IR spectra of the initial ash and the activated samples (Figure 2 in PAPER IV) are characterized by bands at around $1410\ \text{cm}^{-1}$, $873\ \text{cm}^{-1}$ and $712\ \text{cm}^{-1}$ representing C–O stretching and bending of CO_3^{2-} ion [47,48] that show the presence of calcite (and dolomite), also detected in the XRD analysis. The shoulder at $1120\ \text{cm}^{-1}$ and the low-intensity band at $594\ \text{cm}^{-1}$ in the original ash spectrum correspond to the stretching and bending of S–O bond in SO_4^{2-} ion in the sulfate bearing phases (e.g. ettringite) [48].

Changes in the ATR-FT-IR spectra of the activated WHB ash samples (Figure 2 in PAPER IV), show similar features and characteristics, that were observed in activated black ash mixtures. Bands at around $3300\text{--}3400\text{ cm}^{-1}$ and 1640 cm^{-1} , corresponding to O–H stretching and bending vibrations of water, appear in all activated samples due to hydration. In addition, a sharp band at 3640 cm^{-1} , characteristic of O–H stretching in portlandite [$\text{Ca}(\text{OH})_2$], is present [65]. In the water-ash mixtures the main Si–O(–Si/Al) band, centred in the initial ash at 976 cm^{-1} [49], shifts to higher wavenumbers after 28 days of curing, indicating polycondensation of silicate species (PAPER IV). The broad band at 1110 cm^{-1} can be interpreted as a combination of Si–O stretching vibrations from amorphous silicate phases associated with branching Q^3 silicon sites [64] and S–O vibrations of SO_4^{2-} in sulfate minerals.

The NaOH activated ash mixtures (Figure 2 in PAPER IV) show a Si–O (Al) asymmetric stretching vibrations band that after 7 days of curing splits into two components at c. 930 cm^{-1} and c. 980 cm^{-1} . These can be interpreted as Si–O–Al and Si–O–Si stretching vibrations in $\text{Q}^2(1\text{Al})$ and Q^2 silicon site, respectively [51]. The well-defined shape of the 930 cm^{-1} band indicates a crystalline silicate structure (PAPER IV). Its disappearance after 28 days of curing suggests that a reaction period longer than 7 days is needed for the NaOH activation in order to depolymerize the initial silicate structure. An excess of the Ca compared to Si in C–S–H gel formation is evident by the secondary portlandite formation, indicated by appearance of the sharp band at 3640 cm^{-1} (PAPER IV).

The ATR-FT-IR spectra of the WHB ash and sodium silicate based mixtures (Figure 2 in PAPER IV) show the Si–O(–Si/Al) stretching band shifting to lower values of around 960 cm^{-1} after 7 days and then back to higher values of $970\text{--}980\text{ cm}^{-1}$ after 28 days, depicting the initial depolymerization and the subsequent rearrangement of silicate bonds back into polymeric chains and is similar to the shift observed in sodium silicate based mixtures of SHC ash from Petroter type retort (black ash) (PAPER II and IV). The initial shift to lower wavenumbers depicts de-structuring of the silicate units and Al substitution [66,67] and the subsequent shift towards a higher wavenumber corresponds to formation of longer and more interconnected polymeric silicate species [51].

4.3.3. Strength development

The average uniaxial compressive strength of hydrated Enefit280 WHB ash was 3.5 MPa and 3.8 MPa after 7 and 28 days of curing, respectively. In contrast, the WHB ash samples prepared with sodium silicate based solutions achieved typically good results in compressive strength already after 7 days of curing (Figure 4 in PAPER IV). However, Na-silicate based samples show a drop in strength after 28 days, from 7.9 to 6 MPa. Samples prepared with Na-silicate/NaOH solution were significantly stronger. All samples gained strength over the curing period reaching 4.8 and 10 MPa on average, after 7 and 28 days, respectively. The samples prepared with only the NaOH solution did not gain

any significant strength over the curing period and a maximum strength of only 1 MPa was achieved. The compression curves of the material showed high residual strength, indicating that no rigid cementation was developed (Figure 5 in PAPER IV). A brittle behaviour was however observed in all other mixtures, during the curing period.

5. GEOPLOYMERIC POTENTIAL OF ESTONIAN OIL SHALE PROCESSING RESIDUES

Reactive components potentially used for geopolymers represent a wide range of different materials. Typically clay and/or natural pozzolan materials [1] like volcanic ash are considered as primary materials for geopolymeric binders. Also, variety of secondary materials like slags and ashes from different processes can be used. All of these have considerably diverse starting compositions and result in large variety of alkali activation reaction products. The “classical” geopolymers are based on aluminosilicate raw materials such as kaolin clay and/or aluminosilicate fly ashes that form strong aluminosilicate polymer networks upon alkali activation [1]. On the other hand, slags with high CaO content develop cementitious calcium-silicate-hydrate (C–S–H) and calcium-aluminium-hydrate (C–A–H) phases that are formed in ordinary Portland cement hydration [8]. Therefore, to achieve and maintain good strength and chemical resistance/durability of the geopolymeric materials the initial composition and selection of additives and proper activation methods is important.

In general, the composition of the Estonian oil shale ash produced either in thermal power plants or in shale oil retorting processes is considerably different from the raw materials typically used for producing geopolymeric binders (Table 2 in PAPER I, Table 3 in PAPER II, Table 1 in PAPER IV). By its composition oil shale ash could be considered a class C fly ash that is a Ca-rich ash (CaO content >20 wt%), that can be and are used to produce geopolymers with considerable final strength [6,8]. Indeed, the variation of chemical composition of oil shale ashes of different origin [12,13,14,31–35,42] (Table 2 in PAPER I, Table 3 in PAPER II, Table 1 in PAPER IV) agrees (or is somewhat higher) with relative CaO content reported in several other geopolymer raw materials.

Availability of reactive calcium plays an important role in the cementation of TPP and SHC ashes in mixtures with plain water, which is mainly propagated by the formation of secondary Ca–Al–sulfate phases (ettringite) and Ca-carbonate that precipitates upon CaO_{free} (lime) hydration into $\text{Ca}(\text{OH})_2$ (portlandite) and its subsequent carbonation [42]. In both ash types activated with NaOH and Na-silicate, ettringite is absent and Ca-carbonate formation is subdued. ATR-FT-IR and ^{29}Si MAS-NMR analysis of these ashes activated with NaOH, Na-silicate and Na-silicate/NaOH shows that polymerization processes occur. However ^{29}Si MAS-NMR data suggest that the polymerized silicate structures formed in the alkali activation of fresh TPP ashes are one-dimensional and do not contain chain branching $\text{Q}^3(\text{mAl})$ and cross-linking $\text{Q}^4(\text{mAl})$ tetrahedra that are formed in activated SHC ashes (black ash and WHB ash), with the latter feature being characteristic to a three-dimensional geopolymer structure (Figure 1). This is furthermore confirmed by the shift of the main Si–O(–Si/Al) peak (930–980 cm^{-1}) in ATR-FT-IR spectra which shows that longer polymeric chains are formed in SHC ashes. Additionally, SEM-EDS

spectra indicate that the amorphous matrix formed in activated SHC ash contains a notably higher amount of Al (7 wt%) than the phase formed in activated TTP ashes (1 wt%), indicating a higher degree of Al substitution.

However, high Ca content in the oil shale ashes is not a common constituent of a typical geopolymer structure, which is a hydrous alkali aluminosilicate with a tetrahedral silicate network and a number of tetrahedral positions occupied by Al^{3+} in four fold coordination, charge stabilised by an alkali cation [1]. Also, there can be some Al–O–Al groups and non-bridging oxygens of the form Si–OH, $\text{Si–O}^- \text{Na}^+$ or Al–OH existing in the system [56,58]. Nevertheless, Yip et al. [72] has proposed that in the presence of elevated calcium concentrations in geopolymeric system, a C–S–H based cementitious material may form instead. Indeed, as mentioned above, the ^{29}Si MAS-NMR analyses of studied TPP and SHC ash mixtures show that a C–(A)–S–H phase with a chemical shift typical to a system saturated with Na^+ has formed, which is further supported by behaviour of Si–O(–Si/Al) stretching bands in ATR-FT-IR spectra of activated materials.

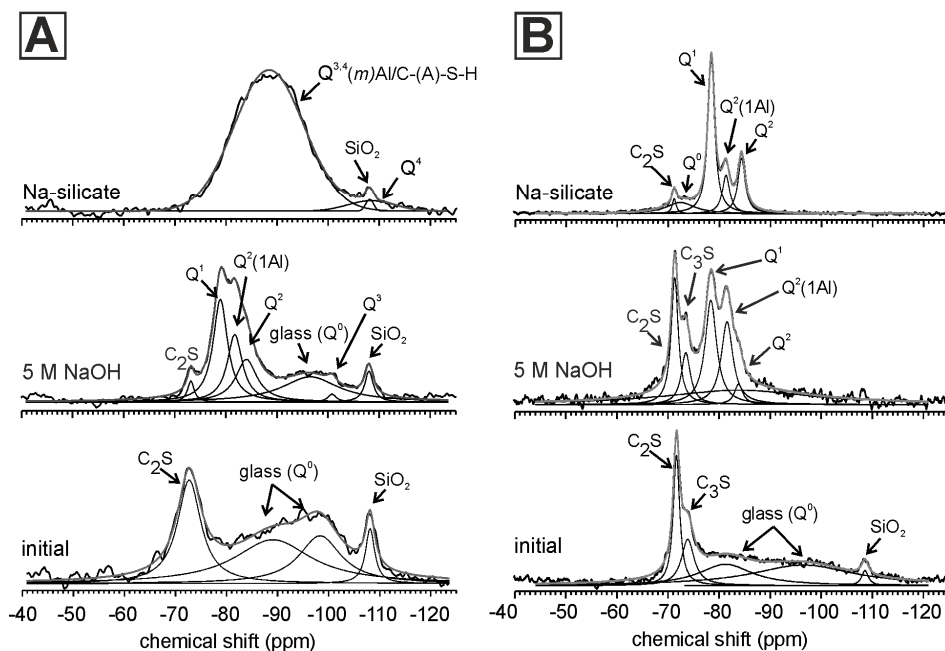


Figure 1. ^{29}Si MAS-NMR spectra of initial unhydrated ash material and Na-silicate and 5M NaOH activated samples after 28 days of curing of (A) black ash and (B) cyclone separator ash (CA). Explanation of $\text{Q}^n(\text{mAl})$ notation on pages 18 and 19.

In addition, several earlier studies [72,73,74] have shown that the CaO in source material used for geopolymerization appears to strengthen the geopolymer by the decrease of microstructural porosity and formation of amorphous Ca–Al–Si gel. The elevated calcium content in the solid raw materials affects the process

of geopolymerization by providing extra nucleation sites for precipitation of dissolved species [75]. In this sense, the presence of high calcium, formation of polymerized C–S–H and C–(A)–S–H gels in activated TPP and retorting ashes would suggest formation of high performance geopolymer. Formation of (Na)-Ca-Al-Si gel is evident from SEM-EDS spectra of amorphous masses in Na-silicate and Na-silicate/NaOH activated samples made with both TPP and SHC ash.

However, excessive calcium and high pH (activity of hydroxide ions) in initial synthesising solution causes precipitation of $\text{Ca}(\text{OH})_2$ (portlandite), which later reacts with CO_2 in the atmosphere forming calcite, resulting in deterioration of the geopolymeric product. This feature is evident in all mixtures based on 5M NaOH. Portlandite also appears in mixtures of TPP ashes prepared with Na-silicate containing activators, but it is absent in SHC based samples. This difference in excess calcium between TPP and SHC results from the amount of reactive Ca-bearing phases in the respective materials.

The initial compressive strengths achieved with sodium silicate based mixtures agree well with the formation of polymeric structures apparent from ^{29}Si MAS-NMR and ATR-FT-IR data. However, though the analysis shows that the polycondensation in Na-silicate and Na-silicate/NaOH activated mixtures is ongoing and the polymerized chains are growing in length, the measured compressive strength values are lower in aged samples (7 days of curing vs. 28 to 90 days of curing). This is evidently due to strong dry shrinkage and formation of abundant micro-cracks observed in the geopolymerized samples, particularly in SHC ash mixtures. Although longer curing times lead to formation of structurally longer and more polymerized aluminosilicate binder phase (PAPERS I, III & IV) and this trend can be expected to continue with time, the coherence of the sample is lost. As a result, though the binder phase itself is at molecular level getting stronger it does not contribute to the increase in mechanical strength of the samples. Dry shrinkage is not observed in samples activated with NaOH, however, this material shows very low initial compressive strength values though the further increase of the strength correlates well with the dissolution and development of the silicate structures in NaOH activated samples.

Shrinkage and creep are a typical processes observed in systems based on cement and geopolymer binders [76] which results mainly from drying shrinkage that can be controlled by selecting optimum curing temperature and liquid-to-ash ratio. Further studies are needed to find optimal conditions for making durable oil shale ash based geopolymers that in principle show good polymerization properties under alkali activation.

Another peculiarity of Estonian oil shale ashes is, compared with other raw materials [77], consistently lower proportion of Al_2O_3 (typically <10 wt%). This compositional characteristic by itself dictates that formation of strong aluminosilicate polymer networks does not contribute or is subdued in development of uniaxial strength. High content of alkali elements (network modifiers), as in oil shale residues, would potentially provide charge-balancing by balancing

the negative charge of tetrahedral aluminium [78]. This makes aluminium stay in 4-coordination, which has higher solubility than the 6-coordination form and as a result more Al would be available for geopolymerization and fly ashes with higher network modifying agents generally produce stronger geopolymers [79]. The network modifier content in all types of oil shale ashes is higher or in the same range as in the raw materials producing the strongest geopolymers. However there is evidently a substantial deficiency of Al, suggesting that in oil shale ashes the development of strength is not limited by the availability of network modifiers, but the low content of potentially soluble silica and specifically aluminium phases.

Overall, this means that for production of geopolymeric materials from oil shale processing wastes, the mix design must include a source of available Si and Al in combination with an appropriate activator mixed at an optimum ratio to induce a sufficient degree of depolymerization-repolymerization reactions.

6. CONCLUSIONS

This thesis focuses on the development of geopolymeric silicate binder phases formed in alkali activated Estonian oil shale solid wastes. That would enable valorisation of the material through its use in different construction or stabilisation applications. The thesis aimed for characterisation of the polymer formation, its structural development and the improvement of cementitious properties of alkali activated materials expressed by the increase of uniaxial compressive strength. The main results of this study show that:

- 1) geopolymerization of Estonian oil shale solid wastes is controlled by the presence and dissolution of reactive Ca-bearing phases. The geopolymeric potential of oil shale ashes is limited by the amount of available Si and Al in the source material. Excess Ca in activated samples is precipitated as portlandite $[(Ca(OH)_2)]$ and its formation shows Si deficiency in the system, with respect to polymer formation. To induce a substantial polymer formation, additional sources of readily available Si and Al must be introduced in the mix design;
- 2) activation with 5M NaOH is not sufficient enough to fully dissolve the amorphous glass phases present in the waste materials and the treatment does not lead to the formation of substantial amounts of polymeric silicate binder phase. The high pH of the system also subdues carbonation reactions and formation of secondary Ca-Al-sulfate phases that are responsible for strength development in hydrated wastes. As a result cementation of activated materials is not developed within 28 days of curing. The lower strength of the NaOH activated mixtures, compared to hydrated samples, is due to suppressed formation of the ettringite/monosulfate phases, that attribute to a large fraction of the early strength of water based mixtures;
- 3) activation of fresh, unhydrated Estonian oil shale solid ash wastes with sodium silicate based activator solutions induces the formation of a polymeric C–(A)–S–H type binder phase that forms an amorphous matrix in the material pore space, filling the area between unreacted ash particles. This feature is however not present in activated ash plateau sediment, which does not contain enough reactive Ca-bearing phases. The activated ash materials show high initial compressive strength values after curing for 7 days. However, already after 7 days, the microstructure of these pore space filling gel-like masses show development of dense microfracturing that penetrates the samples. The fracturing is accompanied by strong dry shrinkage, all resulting in a remarkable drop in compressive strength. The development of the compressive strength in mixtures activated with Na-silicate and Na-silicate/NaOH show different patterns and highest strength values were achieved in WHB and TPP ash mixtures with Na-silicate/NaOH activator and with Na-silicate activator in the case of black ash;

- 4) the C-(A)-S-H phase formed in activated TPP ash is structurally one-dimensional and contains a considerable amount of silica tetrahedra in Q¹ position corresponding to a silicate structure with relatively short chain length. However, Al substituted two-dimensional and three-dimensionally cross-linked structures are formed in activated SHC ashes, showing the formation of stronger geopolymeric phase with significantly longer aluminosilicate chain structure. The structural characteristics of the polymeric phase, however, indicate that SHC type ash is better suited for the production of a geopolymeric material through alkali activation. Nevertheless, for industrial applications, further optimisation of the mix design and curing conditions, possibly including thermal curing, must be undertaken, with emphasis on reduction of dry shrinkage, including microstructural cracking and increase of available Si and Al sources that could possibly be provided through the addition of another industrial waste product.

REFERENCES

1. Davidovits, J.: Geopolymer Chemistry and Applications, 3rd ed. Institut Géopolymère, Saint-Quentin (2011)
2. Duxson, P., Fernandez-Jimenez, A., Provis, J.L., Lukey, G.C., Palomo, A., van Deventer, J.S.J.: Geopolymer technology: the current state of the art. *Journal of Materials Science* **42**(9), 2917–2933 (2007). doi:10.1007/s10853-006-0637-z
3. Li, Q., Xu, H., Li, F.H., Li, P.M., Shen, L.F., Zhai, J.P.: Synthesis of geopolymer composites from blends of CFBC fly and bottom ashes. *Fuel* **97**, 366–372 (2012). doi:10.1016/j.fuel.2012.02.059
4. Subaer, Riessen, A.: Thermo-mechanical and microstructural characterisation of sodium-poly(sialate-siloxo) (Na-PSS) geopolymers. *Journal of Materials Science* **42**(9), 3117–3123 (2006). doi:10.1007/s10853-006-0522-9
5. Zhang, Z.H., Wang, H., Zhu, Y.C., Reid, A., Provis, J.L., Bullen, F.: Using fly ash to partially substitute metakaolin in geopolymer synthesis. *Applied Clay Science* **88–89**, 194–201 (2014). doi:10.1016/j.clay.2013.12.025
6. Guo, X.L., Shi, H.S., Chen, L.M., Dick, W.A.: Alkali-activated complex binders from class C fly ash and Ca-containing admixtures. *Journal of Hazardous Materials* **173**(1–3), 480–486 (2010). doi:10.1016/j.jhazmat.2009.08.110
7. Guo, X.L., Shi, H.S., Dick, W.A.: Compressive strength and microstructural characteristics of class C fly ash geopolymer. *Cement & Concrete Composites* **32**(2), 142–147 (2010). doi:10.1016/j.cemconcomp.2009.11.003
8. Mijarsh, M.J.A., Johari, M.A.M., Ahmad, Z.A.: Effect of delay time and Na₂SiO₃ concentrations on compressive strength development of geopolymer mortar synthesized from TPOFA. *Construction and Building Materials* **86**, 64–74 (2015). doi:10.1016/j.conbuildmat.2015.03.078
9. Bernal, S.A., Rodriguez, E.D., Kirchheim, A.P., Provis, J.L.: Management and valorisation of wastes through use in producing alkali-activated cement materials. *Journal of Chemical Technology and Biotechnology* **91**(9), 2365–2388 (2016). doi:10.1002/jctb.4927
10. Provis, J.L., Palomo, A., Shi, C.J.: Advances in understanding alkali-activated materials. *Cement and Concrete Research* **78**, 110–125 (2015). doi:10.1016/j.cemconres.2015.04.013
11. Bauert, H., Kattai, V.: Kukersite oil shale. In: Raukas, A., Teedumäe, A. (eds.) *Geology and mineral resources of Estonia*. pp. 313–327. Estonian Academy Publishers, Tallinn (1997)
12. Ots, A.: Oil shale fuel combustion. Tallinna Raamatutrükikoda, Tallinn (2006)
13. Bitukova, L., Mötlep, R., Kirsimäe, K.: Composition of Oil Shale Ashes from Pulverized Firing and Circulating Fluidized-Bed Boiler in Narva Thermal Power Plants, Estonia. *Oil Shale* **27**(4), 339–353 (2010). doi: 10.3176/oil.2010.4.07
14. Mötlep, R., Kirsimäe, K., Talviste, P., Puura, E., Jürgenson, J.: Mineral composition of Estonian oil shale semi-coke sediments. *Oil Shale* **24**(3), 405–422 (2007).
15. Siirde, A., Roos, I., Martins, A.: Estimation of Carbon Emission Factors for the Estonian Shale Oil Industry. *Oil Shale* **28**, 127–139 (2011). doi:10.3176/oil.2011.1.S.05
16. World_Energy_Council: World Energy Resources: 2013 Survey. World Energy Council. https://www.worldenergy.org/wp-content/uploads/2013/09/Complete_WER_2013_Survey.pdf (2013)

17. Dyni, J.R.: Oil shale developments in the United States. *Oil Shale* **23**(2), 97–98 (2006).
18. Wang, J.L., Feng, L.Y., Steve, M., Tang, X., Gail, T.E., Mikael, H.: China's unconventional oil: A review of its resources and outlook for long-term production. *Energy* **82**, 31–42 (2015). doi:10.1016/j.energy.2014.12.042
19. Hrayshat, E.S.: Oil Shale – An alternative energy source for Jordan. *Energy Sources Part a-Recovery Utilization and Environmental Effects* **30**(20), 1915–1920 (2008). doi:10.1080/15567030701468175
20. Schmidt, S.J.: New directions for shale oil: Path to a secure new oil supply well into this century [on the example of Australia]. *Oil Shale* **20**(3), 333–346 (2003).
21. World_Energy_Council: World Energy Resources: 2016. World Energy Council. (2016)
22. Kearns, J., Tuohy, E.: Trends in Estonian oil shale utilization: October 2015. International Centre for Defence and Security. <http://www.digar.ee/id/nlib-digar:268094> (2015)
23. Põder, K. (ed.) Statistical Yearbook of Estonia 2016. Statistics Estonia, Tallinn (2016)
24. Pets, L., Knot, P., Haldna, J., Shvenke, G., Juga, R.: Trace elements in kukersite oil shale ash of Baltic Power Plant. *Oil Shale* **2**, 379–390 (1985).
25. Hanni, R.: Energy and valuable material by-product from firing Estonian oil shale. *Waste Management* **16**(1–3), 97–99 (1996). doi: 10.1016/S0956-053x(96)00054-2
26. Kaasik, A., Vohla, C., Mõtsep, R., Mander, Ü., Kirsimäe, K.: Hydrated calcareous oil-shale ash as potential filter media for phosphorus removal in constructed wetlands. *Water Research* **42**(4–5), 1315–1323 (2008). doi: 10.1016/j.watres.2007.10.002
27. Kasak, K., Mõtsep, R., Truu, M., Truu, J., Kõiv-Vainik, M., Espenberg, M., Paiste, P., Kirsimäe, K., Mander, Ü.: Hydrated Oil Shale Ash Mitigates Greenhouse Gas Emissions from Horizontal Subsurface Flow Filters for Wastewater Treatment. *Water Air and Soil Pollution* **227**(9) (2016). doi:10.1007/S11270-016-3007-8
28. Kõiv, M., Liira, M., Mander, Ü., Mõtsep, R., Vohla, C., Kirsimäe, K.: Phosphorus removal using Ca-rich hydrated oil shale ash as filter material – The effect of different phosphorus loadings and wastewater compositions. *Water Research* **44**(18), 5232–5239 (2010). doi: 10.1016/j.watres.2010.06.044
29. Kõiv, M., Ostonen, I., Vohla, C., Mõtsep, R., Liira, M., Lõhmus, K., Kirsimäe, K., Mander, Ü.: Reuse potential of phosphorus-rich filter materials from subsurface flow wastewater treatment filters for forest soil amendment. *Hydrobiologia* **692**(1), 145–156 (2012). doi: 10.1007/s10750-011-0944-5
30. Liira, M., Kõiv, M., Mander, Ü., Mõtsep, R., Vohla, C., Kirsimäe, K.: Active Filtration of Phosphorus on Ca-Rich Hydrated Oil Shale Ash: Does Longer Retention Time Improve the Process? *Environmental Science & Technology* **43**(10), 3809–3814 (2009). doi: 10.1021/Es803642m
31. Pihu, T., Arro, H., Prikk, A., Rootamm, R., Konist, A., Kirsimäe, K., Liira, M., Mõtsep, R.: Oil shale CFBC ash cementation properties in ash fields. *Fuel* **93**(1), 172–180 (2012). doi: 10.1016/j.fuel.2011.08.050
32. Mõtsep, R., Sild, T., Puura, E., Kirsimäe, K.: Composition, diagenetic transformation and alkalinity potential of oil shale ash sediments. *Journal of Hazardous Materials* **184**(1–3), 567–573 (2010). doi: 10.1016/j.jhazmat.2010.08.073

33. Paat, A., Traksmaa, R.: Investigation of the mineral composition of Estonian oil-shale ash using X-ray diffractometry. *Oil Shale* **19**(4), 373–386 (2002).
34. Paat, A.: About the mineralogical composition of Estonian oil shale ash. *Oil Shale* **19**(3), 321–333 (2002).
35. Kuusik, R., Uibu, M., Kirsimäe, K.: Characterization of oil shale ashes formed at industrial-scale CFBC boilers. *Oil Shale* **22**(4), 407–419 (2005).
36. Liira, M., Kirsimäe, K., Kuusik, R., Mõtsep, R.: Transformation of calcareous oil-shale circulating fluidized-bed combustion boiler ashes under wet conditions. *Fuel* **88**(4), 712–718 (2009). doi: 10.1016/j.fuel.2008.08.012
37. Sedman, A., Talviste, P., Kirsimäe, K.: The Study of Hydration and Carbonation Reactions and Corresponding Changes in the Physical Properties of Co-Deposited Oil Shale Ash and Semicoke Wastes in a Small-Scale Field Experiment. *Oil Shale* **29**(3), 279–294 (2012). doi: 10.3176/oil.2012.3.07
38. Siirde, A., Eldermann, M., Rohumaa, P., Gusca, J.: Analysis of Greenhouse Gas Emissions from Estonian Oil Shale Based Energy Production Processes. Life Cycle Energy Analysis Perspective. *Oil Shale* **30**, 268–282 (2013). doi:10.3176/oil.2013.2S.07
39. Aarna, I.: Developments in Production of Synthetic Fuels out of Estonian Oil Shale. *Energy & Environment* **22**(5), 541–552 (2011). doi:10.1260/0958-305X.22.5.541
40. Soone, J., Doilov, S.: Sustainable utilization of oil shale resources and comparison of contemporary technologies used for oil shale processing. *Oil Shale* **20**(3), 311–323 (2003).
41. Golubev, N.: Solid oil shale heat carrier technology for oil shale retorting. *Oil Shale* **20**(3), 324–332 (2003).
42. Talviste, P., Sedman, A., Mõtsep, R., Kirsimäe, K.: Self-cementing properties of oil shale solid heat carrier retorting residue. *Waste Management & Research* **31**(6), 641–647 (2013). doi: 10.1177/0734242x13482033
43. Veiderma, M.: Estonian oil shale – Resources and usage. *Oil Shale* **20**(3), 295–303 (2003).
44. Sedman, A., Talviste, P., Mõtsep, R., Jõelet, A., Kirsimäe, K.: Geotechnical characterization of Estonian oil shale semi-coke deposits with prime emphasis on their shear strength. *Engineering Geology* **131**, 37–44 (2012). doi: 10.1016/j.enggeo.2012.02.002
45. Reinik, J., Heinmaa, I., Mikkola, J.P., Kirso, U.: Hydrothermal alkaline treatment of oil shale ash for synthesis of tobermorites. *Fuel* **86**(5–6), 669–676 (2007). doi:10.1016/j.fuel.2006.09.010
46. Reinik, J., Heinmaa, I., Kirso, U., Kallaste, T., Ritamäki, J., Bostrom, D., Pongracz, E., Huuhtanen, M., Larsson, W., Keiski, R., Kordas, K., Mikkola, J.P.: Alkaline modified oil shale fly ash: Optimal synthesis conditions and preliminary tests on CO₂ adsorption. *Journal of Hazardous Materials* **196**, 180–186 (2011). doi:10.1016/j.jhazmat.2011.09.006
47. Garcia-Lodeiro, I., Fernandez-Jimenez, A., Blanco, M.T., Palomo, A.: FTIR study of the sol-gel synthesis of cementitious gels: C-S-H and N-A-S-H. *Journal of Sol-Gel Science and Technology* **45**(1), 63–72 (2008). doi:10.1007/s10971-007-1643-6
48. Fernández-Carrasco, L., Torrens-Martín, D., Morales, L.M., Martínez-Ramírez, S.: Infrared Spectroscopy in the Analysis of Building and Construction Materials. In: Theophanides, T. (ed.) *Infrared Spectroscopy – Materials Science, Engineering and Technology*. InTech, (2012)

49. Yu, P., Kirkpatrick, R.J., Poe, B., McMillan, P.F., Cong, X.D.: Structure of calcium silicate hydrate (C-S-H): Near-, mid-, and far-infrared spectroscopy. *Journal of the American Ceramic Society* **82**(3), 742–748 (1999).
50. Garbev, K., Stemmermann, P., Black, L., Breen, C., Yarwood, J., Gasharova, B.: Structural features of C-S-H(I) and its carbonation in air – A Raman spectroscopic study. Part I: Fresh phases. *Journal of the American Ceramic Society* **90**(3), 900–907 (2007). doi:10.1111/j.1551-2916.2006.01428.x
51. Lecomte, I., Henrist, C., Liegeois, M., Maseri, F., Rulmont, A., Cloots, R.: (Micro)-structural comparison between geopolymers, alkali-activated slag cement and Portland cement. *Journal of the European Ceramic Society* **26**(16), 3789–3797 (2006). doi:10.1016/j.jeurceramsoc.2005.12.021
52. Lippmaa, E., Mägi, M., Samoson, A., Engelhardt, G., Grimmer, A.R.: Structural studies of silicates by solid state high resolution Si-29 NMR. *Journal of American Chemical Society* **102**, 4889–4893 (1980).
53. Richardson, M., Dodd, V.A., Lenehan, J.J., Conaty, S., O'Kiely, P.: The influence of cement content and water/cement ratio on the durability of portland cement concretes exposed to silage effluent. *Journal of Agricultural Engineering Research* **72**(2), 137–143 (1999). doi: 10.1006/jaer.1998.0355
54. Richardson, I.G., Groves, G.W.: The Incorporation of Minor and Trace-Elements into Calcium Silicate Hydrate (C-S-H) Gel in Hardened Cement Pastes. *Cement and Concrete Research* **23**(1), 131–138 (1993). doi: 10.1016/0008-8846(93)90143-W
55. Puertas, F., Palacios, M., Manzano, H., Dolado, J.S., Rico, A., Rodriguez, J.: A model for the C-A-S-H gel formed in alkali-activated slag cements. *Journal of the European Ceramic Society* **31**(12), 2043–2056 (2011). doi:10.1016/j.jeurceramsoc.2011.04.036
56. Sun, G.K., Young, J.F., Kirkpatrick, R.J.: The role of Al in C-S-H: NMR, XRD, and compositional results for precipitated samples. *Cement and Concrete Research* **36**(1), 18–29 (2006). doi:10.1016/j.cemconres.2005.03.002
57. Andersen, M.D., Jakobsen, H.J., Skibsted, J.: Characterization of white Portland cement hydration and the C-S-H structure in the presence of sodium aluminate by Al-27 and Si-29 MAS NMR spectroscopy. *Cement and Concrete Research* **34**(5), 857–868 (2004). doi:10.1016/j.cemconres.2003.10.009
58. Faucon, P., Delagrave, A., Petit, J.C., Richet, C., Marchand, J.M., Zanni, H.: Aluminum incorporation in calcium silicate hydrates (C-S-H) depending on their Ca/Si ratio. *Journal of Physical Chemistry B* **103**(37), 7796–7802 (1999). doi: 10.1021/Jp990609q
59. Taylor, H.F.W.: *Cement Chemistry*, 2nd Edition ed. Thomas Telford Ltd, London (1997)
60. Richardson, I.G.: The nature of the hydration products in hardened cement pastes. *Cement & Concrete Composites* **22**(2), 97–113 (2000). doi: 10.1016/S0958-9465(99)00036-0
61. Richardson, I.G.: Tobermorite/jennite- and tobermorite/calcium hydroxide-based models for the structure of C-S-H: applicability to hardened pastes of tricalcium silicate, beta-dicalcium silicate, Portland cement, and blends of Portland cement with blast-fumace slag, metakaolin, or silica fume. *Cement and Concrete Research* **34**(9), 1733–1777 (2004). doi:10.1016/j.cemconres.2004.05.034
62. Allen, A.J., Thomas, J.J., Jennings, H.M.: Composition and density of nanoscale calcium-silicate-hydrate in cement. *Nature Materials* **6**(4), 311–316 (2007). doi:10.1038/nmat1871

63. Rodriguez, E.T., Richardson, I.G., Black, L., Boehm-Courjault, E., Nonat, A., Skibsted, J.: Composition, silicate anion structure and morphology of calcium silicate hydrates (C-S-H) synthesised by silica-lime reaction and by controlled hydration of tricalcium silicate (C3S). *Advances in Applied Ceramics* **114**(7), 362–371 (2015). doi:10.1179/1743676115Y.0000000038
64. Rees, C.A., Provis, J.L., Lukey, G.C., van Deventer, J.S.J.: In situ ATR-FTIR study of the early stages of fly ash geopolymer gel formation. *Langmuir* **23**(17), 9076–9082 (2007). doi:10.1021/la701185g
65. Lodeiro, I.G., Macphee, D.E., Palomo, A., Fernandez-Jimenez, A.: Effect of alkalis on fresh C-S-H gels. FTIR analysis. *Cement and Concrete Research* **39**(3), 147–153 (2009). doi:10.1016/j.cemconres.2009.01.003
66. Hajimohammadi, A., Provis, J.L., van Deventer, J.S.J.: One-Part Geopolymer Mixes from Geothermal Silica and Sodium Aluminate. *Industrial & Engineering Chemistry Research* **47**(23), 9396–9405 (2008). doi:10.1021/ie8006825
67. Lee, W.K.W., van Deventer, J.S.J.: Use of infrared spectroscopy to study geopolymerization of heterogeneous amorphous aluminosilicates. *Langmuir* **19**(21), 8726–8734 (2003). doi:10.1021/la026127e
68. Mägi, M., Lippmaa, E., Samoson, A., Engelhardt, G., Grimmer, A.R.: Solid-state high-resolution silicon-29 chemical shifts in silicates. *Journal of Physical Chemistry* **88**, 1518–1522 (1984).
69. Faucon, P., Petit, J.C., Charpentier, T., Jacquinot, J.F., Adenot, F.: Silicon substitution for aluminum in calcium silicate hydrates. *Journal of the American Ceramic Society* **82**(5), 1307–1312 (1999).
70. Garcia-Lodeiro, I., Fernandez-Jimenez, A., Sobrados, I., Sanz, J., Palomo, A.: C-S-H Gels: Interpretation of Si-29 MAS-NMR Spectra. *Journal of the American Ceramic Society* **95**(4), 1440–1446 (2012). doi:10.1111/j.1551-2916.2012.05091.x
71. Lodeiro, I.G., Fernandez-Jimenez, A., Palomo, A., Macphee, D.E.: Effect on fresh C-S-H gels of the simultaneous addition of alkali and aluminium. *Cement and Concrete Research* **40**(1), 27–32 (2010). doi:10.1016/j.cemconres.2009.08.004
72. Yip, C.K., Lukey, G.C., van Deventer, J.S.J.: The coexistence of geopolymeric gel and calcium silicate hydrate at the early stage of alkaline activation. *Cement and Concrete Research* **35**(9), 1688–1697 (2005). doi:10.1016/j.cemconres.2004.10.042
73. Komnitsas, K.A.: Potential of geopolymer technology towards green buildings and sustainable cities. 2011 International Conference on Green Buildings and Sustainable Cities **21**, 1023–1032 (2011). doi:10.1016/j.proeng.2011.11.2108
74. Xu, H., Van Deventer, J.S.J.: The geopolymerisation of aluminosilicate minerals. *International Journal of Mineral Processing* **59**(3), 247–266 (2000). doi:http://dx.doi.org/10.1016/S0301-7516(99)00074-5
75. van Deventer, J.S.J., Provis, J.L., Duxson, P., Lukey, G.C.: Reaction mechanisms in the geopolymeric conversion of inorganic waste to useful products. *Journal of Hazardous Materials* **139**(3), 506–513 (2007). doi:http://dx.doi.org/10.1016/j.jhazmat.2006.02.044
76. Castel, A., Foster, S.J., Ng, T., Sanjayan, J.G., Gilbert, R.I.: Creep and drying shrinkage of a blended slag and low calcium fly ash geopolymer Concrete. *Materials and Structures*, 1–10 (2015). doi:10.1617/s11527-015-0599-1
77. Provis, J.L., Bernal, S.A.: Geopolymers and Related Alkali-Activated Materials. *Annu Rev Mater Res* **44**, 299–327 (2014). doi:10.1146/annurev-matsci-070813-113515

78. Duxson, P., Provis, J.L.: Designing Precursors for Geopolymer Cements. *Journal of the American Ceramic Society* **91**(12), 3864–3869 (2008). doi:10.1111/j.1551-2916.2008.02787.x
79. Aughenbaugh, K.L., Williamson, T. and Juenger, M.C.G.: Critical evaluation of strength prediction methods for alkali-activated fly ash. *Materials and Structures*, **48**(3), 607–620 (2015). doi: 10.1617/s11527-014-0496-z

SUMMARY IN ESTONIAN

Eesti põlevkivitööstuse tahked jäätmed geopolümeeride toormena

Käesoleva doktoritöö eesmärgiks on selgitada Eesti põlevkivitööstuses tekkinud tahkete jäätmete sobivus geopolümeersete materjalide valmistamiseks leelisaktiivisatsiooni meetodil. Geopolümeerid on anorgaaniliste polümeeride hulka kuuluvad tsementeeruvad materjalid, mis moodustuvad alumosilikaatide leelisaktiivisatsioonis. Leeliselises keskkonnas toimub algsete alumosilikaatsete struktuuride depolümeriseerumine, mille tulemusel vabanevad lahusesse reaktiivsed räni ja alumiiniumi ühendid. Nende polükondensatsioonil moodustuvad kolmedimensionaalse kaugstruktuuriga amorfseid alumosilikaatse koostisega tsementeeruvad faasid – geopolümeerid [1].

Geopolümeerid sideained ja nendest valmistatud betoon on oma omadustelt võrreldavad või keemiliselt agressiivsetes keskkondades isegi püsivamad, kui tavalise portlandtsemendi baasil valmistatud analoogid [2]. Geopolümeeride valmistamiseks on toormena võimalik kasutada erinevaid looduslikke- või tehisklikke alumosilikaatseid toormeid. Samas mõjutavad algmaterjali koostis ja aktiivisatsioonitingimused olulisel määral tekkiva geopolümeerse faasi omadusi ning mikrostruktuuri.

Tööstusjäätmete taaskasutamine tsementeeruvate geopolümeersete ja leelisaktiveeritud materjalide toormena võimaldab neid jäätmeid vääridada ning vähendada ladustatavate jäätmete keskkonnamõju [9,10]. Siiani on tööstusjäätmetest peamiselt taaskasutatud alumiiniumitööstuse räbu, klaasitööstuse jääke ning madala Ca sisaldusega ehk F-tüüpi lendtuhkasid, kuid viimase kümnendi uuringud on näidanud ka C-tüüpi kõrge Ca sisaldusega ($\text{CaO} > 20$ massi%) tuhade sobivust geopolümeeride toormeks [6,8]. Lisaks geopolümeersele alumosilikaatsele faasile, võib kõrge Ca sisaldusega algmaterjali aktiveerimisel tekkida polümeerne kaltsium-silikaat-hüdraat (C–S–H), mis on sarnane hüdratiseerunud portlandtsemendis tekkivale tsementeerivale faasile [8] ning kaltsium-alumiinium-silikaat-hüdraat (C–A–S–H) faas [72,73,74], mis parandavad polümeriseeruva materjali tsementeeruvust ja tõstavad lõpptugevust.

Eesti kukersiitne põlevkivi on hetkel maailma enim ekspluateeritud põlevkiviresurss [21]. Põlevkivi kaevandusmahud on viimastel aastatel olnud 18.1–21.5 miljonit tonni aastas [23], millest enamus (~80%) põletatakse soojus- ja elektri- jaamades ning ülejäänust toodetakse põlevkiviõli ja -gaasi [12]. Suure tuhasuse (40–50%) tõttu tekib põlevkivi termilisel töötlemisel Eestis igal aastal 7–8 Mt põlevkivituhka ja ~1 Mt õlitööstuse jäätmeid [23]. Põlevkivituhale on siiani leitud vaid minimaalset taaskasutust (kuni 5%) ja enamik jäätmetest ladestatakse tuhaväljadele. Praegu puudub aga igasugune taaskasutus õlitööstuse jäätmetele, mis ladestatakse täies mahus jäätmehoiulatesse [13,14].

Geopolümeeride tootmine elektri- jaamade ja õlitööstuse tuhasta võiks potentsiaalselt avada täiesti uue võimaluse nende jäätmete taaskasutuseks. Koostiselt võib nii elektri- jaamade kui ka õlitööstuse tuha klassifitseerida C-tüüpi lend-

tuhaks, mis loob varasemate uuringute alusel [6,8] head eeldused selle jäätme võimalikuks väärimiseks geopolümeerse sideainena.

Käesolevas doktoritöös selgitatakse Eesti põlevkivitööstuse tahkete jäätmete omadused ja nende sobivus geopolümeeride valmistamiseks. Uuritava materjalina kasutati erinevaid põlevkivitööstuse jäätmeid: Eesti Energia AS Balti soojuselektrijaama tolmpõletuskatelde tsüklon-separaatori (CA) ja kolde põhjatuhka (BA) ning sama elektrijaama tuhaplatoolt kogutud hüdratiseerunud põlevkivituha setendit (APS) (ARTIKKEL I); Viru Keemia Grupp AS Petrotertüüpi tahke soojuskandja (SHC) põlevkiviõli retordi värsket jäädet (nn must tuhk) (ARTIKKEL II, III); Eesti Energia Enefit280-tüüpi SHC põlevkiviõli retordi hüdratiseerumata jääksoojuskatla (WHB) tuhka (ARTIKKEL IV).

Geopolümerisatsiooni esile kutsumiseks aktiveeriti kõiki materjale 5M NaOH, Na-silikaadi ja NaOH lisamisega modifitseeritud Na-silikaadi (Na-silikaat/NaOH) lahustega. Sideaineliste omaduste võrdluseks ning polümerisatsiooniprotsesside ulatuse hindamiseks valmistati kõigist materjalidest paralleelsed katsesegud veega.

Uuringu spetsiifilised eesmärgid olid:

- hinnata erinevate leeliselisaktivaatorite mõju geopolümerisatsiooni-protsessidele;
- tuvastada aktivisatsioonil toimuvate polümerisatsioonireaktsioonide ja reaktsiooniproduktide struktuursed, keemilised ja mineraalsed karakteristikud;
- hinnata tsementatsiooni kujunemise dünaamikat aktiveeritud materjalides ja selgitada muutused tsementeeruva materjali mikrostruktuuris.

Käesoleva uuringu põhitulemused olid järgmised:

- 1) Eesti põlevkivitööstuse tahkete jäätmete geopolümerisatsiooni kontrollib materjalis leiduvate reaktiivsete kaltsiumit sisaldavate faaside sisaldus ja nende lahustumine. Peamiseks geopolümerisatsiooni limiteerivaks faktoriks on aktivisatsioonil lahustuva ja reaktsioonideks vabalt kättesaadava räni ja alumiiniumi madal sisaldus lähtematerjalis. Polümeerse faasi formeerumisest üle jääv liigne kaltsium sadestub aktiveeritud materjalides portlandiidi $[Ca(OH)_2]$ kujul, mis näitab, et polümeriseerumise süsteemis on lahustuva räni defitsiit. Selleks, et indutseerida tuhamaterjalides laialdast polümeerse faasi teket, on vaja lähtematerjalidele lisada aktivatsioonil lahustuvaid komponente, mis tõstaks polümerisatsioonireaktsioonideks kasutatava räni ja alumiiniumi sisaldust.
- 2) Kõrge molaarsusega (5M) NaOH lahusega aktivisatsioon ei ole piisav, et lahustada kogu algmaterjalis leiduv amorfne klaasifaas ja protsessi käigus ei moodustu piisavalt sekundaarset tsementeeruvat polümeerset silikaatset faasi. Samas pärsib süsteemi kõrge pH olulisel määral sekundaarsete Ca-Al sulfaatide tekkimist ja portlandiidi karboniseerumist, mis tüüpiliselt kontrollivad tsementatsiooni veega hüdratiseerunud tuhamaterjalides. Selle tulemusena ei arene Na-hüdroksiidiga aktiveeritud tuhkaades tsementatsiooni ka peale 28-päevast hüdratiseerumist ning materjalid jäävad plastseks. Kõigi

veega hüdratiseeritud tuhade survetugevus oli kogu tsementatsiooni-perioodil kõrgem, kui NaOH-ga aktiveeritud materjalidel.

- 3) Tuhamaterjalide aktiveerimisel naatriumsilikaati (Na_2SiO_3) sisaldavate lahustega moodustub polümeerne C-(A)-S-H-tüüpi tsementeeriv faas. Tekkiv amorfne geeljas mass täidab lausaliselt osakestevahelist pooriruumi. Sellist tüüpi tsementatsioon ei teki aga hüdratiseerunud põlekivituha sette baasil valmistatud proovides, mis näitab, et tuhaplatoo sete ei sisalda piisaval määral reaktiivseid mineraalseid faase, mille lahustumisel vabanev Ca saaks reageerida aktivaatorlahuses sisalduva räniga ja moodustada polümeerseid sideaineid. Tänu tsementeeruva faasi tekkele, omandavad lahustuva silikaadiga aktiveeritud tuhasegud juba seitsme päeva möödudes kõrge survetugevuse. Samas tekib juba seitsme päeva möödudes pooriruumi täitva amorfse faasi maatriksisse ulatuslike mikrolõhede süsteem, millega kaasneb ka proovikehade mõõtmete märgatav kahanemine (kuni 10% ulatuses). Kahanemise ja mikrolõhede tekkimisega kaasneb oluline proovikehade survetugevuses vähenemine kogu ülejäänud tsementatsiooni-perioodi jooksul. Na-silikaadi ja Na-silikaat/NaOH lahustega valmistatud proovikehade survetugevuste dünaamika selgitamine näitas tuhamaterjalide lõikes erinevaid käitumismustreid ning WHB, BA ja CA tuhade puhul saavutati kõrgeimad survetugevuse väärtused Na-silikaat/NaOH ning musta tuha puhul Na-silikaadi aktivaatoriga.
- 4) Soojuselektrijaamade ja õlitootmise tuhkaades moodustunud C-(A)-S-H faasid on struktuurselt erinevad. Aktiveeritud soojuselektrijaamade tuhkaades moodustunud geeljas faas on struktuurselt ühedimensionaalne ja sisaldab olulisel määral polümeerse räniahela otstes paiknevaid või räni-dimeere moodustavaid räni tetraeedreid, mis näitab, et tekkinud silikaatne struktuur koosneb lühikestest ahelatest. Õlitootmise tahke soojuskandja tuhkaades moodustunud faas sisaldab seevastu olulisel määral alumiiniumiga asendunud Si-tetraeedreid, mis näitab kahedimensionaalse ahelstruktuuri ja kolmedimensionaalselt ühendatud geopolümeerse struktuuri teket, mille ahelad on olulisel määral pikemad, võrreldes elektrijaamade tuha aktiveerimisel tekkinud struktuuridega. Kuna polümeersete ahelate pikkus on otseselt seotud struktuuri tugevusega, võib selle alusel väita, et SHC-tüüpi tuhkaades tekkiv faas on paremate sideaineliste omadustega.

Käesoleva uuringu tulemused näitavad, et tuhaplatoodele ladestatud materjali leelisaktiivatsioonil ei teki sekundaarseid polümeerseid räni faase ning seega ei ole see sobilik geopolümeersete materjalide valmistamiseks. Polümeersete tsementeeruvate faaside teke toimub aga elektrijaamade ja õlitööstuse värskete tuhade aktiveerimisel.

Pikkade ahelate ja geopolümeeridele omase kolmedimensionaalse alumsilikaatse struktuuri tekkimise alusel sobivad uuritud tahketest jäätmetest leelisaktiivatsiooni geopolümeersete materjalide valmistamiseks kõige paremini SHC tuhad. Tööstuslike rakenduste välja töötamiseks on vaja täiendavaid uurin-guid, mis keskenduksid optimaalsete seguvahekordade ja tsementatsiooni-

tingimuste välja selgitamisele. Selleks saab kasutada polümerisatsiooni intensiivistamist madalatemperatuurilise termilise töötlemise käigus, aktiveeritud materjalide mahu kahanemise ja mikrostruktuuri lõhelisuse kontrollimist segude koostise ja kivistumiskeskkondade optimeerimisega ja materjali aktivisatsioonil vabaneva Si ja Al allikate osakaalu tõstmist, mida võib olla võimalik saavutada mõne teise tööstusliku jäätme lisamisega.

ACKNOWLEDGEMENTS

First and foremost I would like to express my utmost gratitude to my supervisors. I would also like to thank all co-authors of the papers and all the students and staff at the department of geology who helped with laboratory work, analysis and interpretation of the results and furthermore extend my gratitude to my wife for her support and patience. Financial support from the Doctoral School of Earth Sciences and Ecology and Archimedes Foundation (Kristjan Jaak Scholarship) are gratefully acknowledged.

PUBLICATIONS

CURRICULUM VITAE

Name: Päärn Paiste
Date of birth: 28.07.1987
Address: Department of Geology, University of Tartu,
Ravila 14a, 50411 Tartu, Estonia
Contact: Phone +372 53967592
E- mail: paarn.paiste@ut.ee

Education

2012–... University of Tartu, Department of Geology
PhD student in Geology
2010–2012 University of Tartu, MSc in geology
2006–2009 University of Tartu, BSc in geology

Professional employment

2016– ... Program manager of Geology and Environmental technology
BSc and MSc programs, University of Tartu, Faculty of Science
and Technology
2016– ... Specialist, University of Tartu, Department of Geology
2012– 2015 Specialist, University of Tartu, Department of Geology
2011– 2012 Laboratory technician, University of Tartu, Department of
Geology

Field of research:

geochemistry, valorisation of Estonian oil shale solid wastes, inductively
coupled plasma mass spectrometry

Publications

1. Willmore, A.A., Simon-Gracia, L., Toome, K., **Paiste, P.**, Kotamraju, V.R., Mölder, T., Sugahara, K.N., Ruoslahti, E., Braun, G.B., Teesalu, T., (2016) Targeted silver nanoparticles for radiometric cell phenotyping. *Nanoscale* 8, 9096–9101
2. Joosu, L., Lepland, A., Kreitsmann, T., Üpraus, K., Roberts, N.M.W., **Paiste, P.**, Martin, A.P., Kirsimäe, K., (2016) Petrography and the REE-composition of apatite in the Paleoproterozoic Pilgijärvi Sedimentary Formation, Pechenga Greenstone Belt, Russia. *Geochimica et Cosmochimica Acta* 186, 135–153
3. Kasak, K., Mõtsep, R., Truu, M., Truu, J., Kõiv-Vainik, M., Espenberg, M., **Paiste, P.**, Kirsimäe, K., Mander, Ü. (2016) Hydrated oil shale ash mitigates greenhouse gas emissions from horizontal subsurface flow filters for wastewater treatment. *Water, Air & Soil Pollution* 227:320

4. **Paiste, P.**, Liira, M., Heinmaa, I., Vahur, S., Kirsimäe, K. (2016) Alkali activated construction materials: Assessing the alternative use for oil shale processing solid wastes. *Construction and Building Materials* 122, 458– 464
5. Paaver, P., **Paiste, P.**, Kirsimäe, K. (2016) Geopolymeric potential of the Estonian oil shale solid residues: Petroter solid heat carrier retorting ash. *Oil Shale* 33, 373–392
6. Taal, I., Rohtla, M., Saks, L., Kesler, M., Jürgens, K., Svigsden, R., Matetski, L., Verliin, A., **Paiste, P.**, Vetemaa, M. (2017) Parr dispersal between streams *via* a marine environment: A novel mechanism behind straying for anadromous brown trout? *Ecology of Freshwater Fish* 00, 1–7
7. Jäger, R., Härk, E., Kasatkin, P.E., Pikma, P., Joost, U., **Paiste, P.**, Aruväli, J., Kallio, T., Jian, H., Lust E. (2017) Carbide Derived Carbon Supported Pt Nanoparticles with Optimum Size and Amount for Efficient Oxygen Reduction Reaction Kinetics *Journal of The Electrochemical Society* 164, F448–F453
8. **Paiste, P.**, Külaviir, M., Paaver, P., Heinmaa, I., Vahur, S., Kirsimäe, K. (2017) Beneficiation of oil shale processing waste: secondary binder phases in alkali activated composites. *Waste and Biomass Valorisation*, submitted, in review
9. **Paaver, P.**, Paiste, P., Mõtsep, R., Kirsimäe, K. (2017) Self-cementation properties and alkali activation of Enefit280 solid heat carrier retorting ash. *Oil Shale*, 34, in press.

ELULOOKIRJELDUS

Nimi: Päärn Paiste
Sünniaeg: 28.07.2987
Aadress: Geoloogia osakond, Tartu Ülikool,
Ravila 14a, 50411 Tartu, Eesti
Kontakt: Tel. +372 53967592
E-post: paarn.paiste@ut.ee

Haridus

2012–... Tartu Ülikool, Geoloogia osakond, Geoloogia doktorant
2010–2012 Tartu Ülikool, MSc geoloogias
2006–2009 Tartu Ülikool, BSc geoloogias

Teenistuskäik

2016– ... Geoloogia ja keskkonnatehnoloogia BSc ja MSc õppekavade
programmijuht, Tartu Ülikool, Loodus- ja täppiseaduste
valdkonna dekanat
2016– ... Spetsialist, Tartu Ülikool, Geoloogia osakond
2012– 2015 Spetsialist, Tartu Ülikool, Geoloogia osakond
2011– 2012 Laborant, Tartu Ülikool, Geoloogia osakond

Teadustöö põhisuunad:

Geokeemia, Eesti põlevkivitööstuse tahkete jäätmete väärindamine, induktiiv-
sidesstatud plasma massispektromeetria

Publikatsioonid

1. Willmore, A.A., Simon-Gracia, L., Toome, K., **Paiste, P.**, Kotamraju, V.R., Mölder, T., Sugahara, K.N., Ruoslahti, E., Braun, G.B., Teesalu, T., (2016) Targeted silver nanoparticles for radiometric cell phenotyping. *Nanoscale* 8, 9096–9101
2. Joosu, L., Lepland, A., Kreitsmann, T., Üpraus, K., Roberts, N.M.W., **Paiste, P.**, Martin, A.P., Kirsimäe, K., (2016) Petrography and the REE-composition of apatite in the Paleoproterozoic Pilgijärvi Sedimentary Formation, Pechenga Greenstone Belt, Russia. *Geochimica et Cosmochimica Acta* 186, 135–153
3. Kasak, K., Mõtlep, R., Truu, M., Truu, J., Kõiv-Vainik, M., Espenberg, M., **Paiste, P.**, Kirsimäe, K., Mander, Ü. (2016) Hydrated oil shale ash mitigates greenhouse gas emissions from horizontal subsurface flow filters for wastewater treatment. *Water, Air & Soil Pollution* 227:320
4. **Paiste, P.**, Liira, M., Heinmaa, I., Vahur, S., Kirsimäe, K. (2016) Alkali activated construction materials: Assessing the alternative use for oil shale processing solid wastes. *Construction and Building Materials* 122, 458– 464

5. Paaver, P., **Paiste, P.**, Kirsimäe, K. (2016) Geopolymeric potential of the Estonian oil shale solid residues: Petroter solid heat carrier retorting ash. *Oil Shale* 33, 373–392
6. Taal, I., Rohtla, M., Saks, L., Kesler, M., Jürgens, K., Svigsden, R., Matetski, L., Verliin, A., **Paiste, P.**, Vetemaa, M. (2017) Parr dispersal between streams *via* a marine environment: A novel mechanism behind straying for anadromous brown trout? *Ecology of Freshwater Fish* 00, 1–7
7. Jäger, R., Härk, E., Kasatkin, P.E., Pikma, P., Joost, U., **Paiste, P.**, Aruväli, J., Kallio, T., Jian, H., Lust E. (2017) Carbide Derived Carbon Supported Pt Nanoparticles with Optimum Size and Amount for Efficient Oxygen Reduction Reaction Kinetics *Journal of The Electrochemical Society* 164, F448–F453
8. **Paiste, P.**, Külaviir, M., Paaver, P., Heinmaa, I., Vahur, S., Kirsimäe, K. (2017) Beneficiation of oil shale processing waste: secondary binder phases in alkali activated composites. *Waste and Biomass Valorisation* submitted, in review
9. **Paaver, P.**, Paiste, P., Mõtlep, R., Kirsimäe, K. (2017) Self-cementation properties and alkali activation of Enefit280 solid heat carrier retorting ash. *Oil Shale* 34, in press.

DISSERTATIONES GEOLOGICAE UNIVERSITATIS TARTUENSIS

1. **Пээп Мянник.** Конодонты в верхнеордовикских и нижнесилурийских отложениях Эстонии. Тарту, 1992, 355 с.
2. **Elvi Tavast.** Fennoskandia kilbi lõunanõlva ja sellega piirnevate alade aluspõhja reljeef. Tartu, 1992, 357 lk.
3. **Kaarel Orviku.** Characterisation and evolution of Estonian seashores. Tartu, 1992, 19 p.
4. **Анатолий Молодьков.** ЭПР-анализ скелетного вещества моллюсков в хроностратиграфических исследованиях позднего кайнозоя. Тарту, 1992, 33 с.
5. **Jaan Lutt.** Late- and postglacial deposits on the Estonian shelf. Tartu, 1993, 31 p.
6. **Reet Karukäpp.** Gotiglatsiaalne morfogenees Skandinaavia mandriliustiku kagusektoris. Tartu, 1997, 181 p.
7. **Argo Jõelet.** Geothermal studies of the Precambrian basement and Phanerozoic sedimentary cover in Estonia and Finland. Tartu, 1998, 125 p.
8. **Jüri Nemliher.** Mineralogy of Phanerozoic skeletal and sedimentary apatites: an XRD study. Tartu, 1999, 134 p.
9. **Kalle Kirsimäe.** Clay mineral diagenesis on the Lower Cambrian “Blue Clay” in the northern part of the Baltic Paleobasin. Tartu, 1999, 113 p.
10. **Jüri Plado.** Gravity and magnetic signatures of meteorite impact structures. Tartu, 2000, 87 p.
11. **Olev Vinn.** Morphogenesis and phylogenetic relationships of Clitambonitidines, Ordovician Brachiopods. Tartu, 2001, 127 p.
12. **Leho Ainsaar.** The middle Caradoc facies and faunal turnover in the late Ordovician Baltoscandian palaeobasin: sedimentological and carbon isotope aspects. Tartu, 2001, 109 p.
13. **Oive Tinn.** Early Ostracode evolution and Palaeoenvironmental application in the Ordovician of Baltoscandia. Tartu, 2002, 145 p.
14. **Maris Rattas.** Subglacial environments in the formation of drumlins — The case of the Saadjärve Drumlin Field, Estonia. Tartu, 2004, 117 p.
15. **Ene Kadastik.** Upper-Pleistocene stratigraphy and deglaciation history in northwestern Estonia. Tartu, 2004, 129 p.
16. **Helje Pärnaste.** Early Ordovician trilobites of suborder Cheirurina in Estonia and NW Russia: systematics, evolution and distribution. Tartu, 2004, 138 p.
17. **Mari-Ann Mõtus.** Silurian (Llandovery-Wenlock) tabulate corals of Baltoscandia: taxonomy, palaeoecology, distribution. Tartu, 2005, 167 p.
18. **Alar Rosentau.** Development of proglacial lakes in Estonia. Tartu, 2006, 114 p.
19. **Evelin Verš.** Development of impact-induced hydrothermal system at Kärddla impact structure. Tartu, 2006, 96 p.

20. **Sigitas Radzevičius.** The genus *Pristiograptus* in wenlock of East Baltic and the Holy Cross Mountains. Tartu, 2007, 133 p.
21. **Andres Marandi.** Natural chemical composition of groundwater as a basis for groundwater management in the Cambrian-Vendian aquifer system in Estonia. Tartu, 2007, 116 p.
22. **Eve Niinemets.** Vegetation and land-use history of the Haanja Heights (SE-Estonia) during the holocene. Tartu, 2008, 146 p.
23. **Kalle-Mart Suuroja.** Geology and lithology of the early palaeozoic marine impact structures Kärddla and Neugrund (Estonia). Tartu, 2008, 234 p.
24. **Rutt Hints.** Early diagenesis of Ordovician and Silurian Bentonites in the Northern Baltic Palaeobasin. Tartu, 2009, 90 p.
25. **Peeter Somelar.** Illitization of K-bentonites in the Baltic Basin. Tartu, 2009, 118 p.
26. **Ulla Preeden.** Remagnetizations in sedimentary rocks of Estonia and shear and fault zone rocks of southern Finland. Tartu, 2009, 121 p.
27. **Kati Tänavsuu-Milkeviciene.** Transgressive to regressive turnaround in the Middle Devonian Baltic Basin. Tartu, 2009, 106 p.
28. **Valle Raidla.** Chemical and isotope evolution of groundwater in the Cambrian-Vendian aquifer system in Estonia. Tartu, 2010, 134 p.
29. **Kadri Sohar.** Quaternary ostracods from Estonia and their application in palaeoenvironmental reconstruction. Tartu, 2010, 140 p.
30. **Kristjan Urtson.** Stepwise melt transport and accumulation: analogue and numerical modelling approach. Tartu, 2011, 83 p.
31. **Marko Kohv.** Landslides in clayey soils of western Estonia. Tartu, 2011, 116 p.
32. **Nele Muttik.** Post-impact alteration of impactites: Ries crater, Germany. Tartu, 2011, 78 p.
33. **Annette Sedman.** Strength and self-cementing properties of oil shale retorting wastes. Tartu, 2013, 82 p.
34. **Arkady Tsyrlnikov.** Complex seismo-acoustic and lithological study of the Lateglacial and postglacial sediments northern Gulf of Riga, eastern branch of the central Baltic Sea. Tartu, 2013, 102 p.
35. **Marge Uppin.** Geological sources and hydrochemistry of fluoride and boron in Silurian-Ordovician aquifer system. Tartu, 2013, 86 p.
36. **Peeter Talviste.** Temporal changes in weak natural and artificial soils – influence on geotechnical characteristics. Tartu, 2014, 204 p.
37. **Katrin Lasberg.** Chronology of the Weichselian Glaciation in the south-eastern sector of the Scandinavian Ice Sheet. Tartu, 2014, 100 p.
38. **Sirle Liivamägi.** Neoproterozoic Baltic paleosol: geology and paleoenvironmental interpretation. Tartu, 2015, 94 p.
39. **Lauri Joosu.** Petrography and the rare earth element composition of apatite in 2 Ga Onega and Pechenga basins, Russia: the environmental settings for phosphogenesis. Tartu, 2015, 139 p.
40. **Liisa Lang.** Baculate shell structure in Early Palaeozoic linguliform brachiopods. Tartu, 2015, 114 p.